Dancing Sprites Above a Lightning Mapping Array -an Analysis of the Storm and Flash/Sprite Developments

Maja Tomicic, Serge Soula, Eric Defer, Serge Prieur, Janusz Mlynarczyk, Thomas Farges, Olivier Chanrion, Christoph Köhn, Torsten Neubert

Dancing Sprites Above a Lightning Mapping Array - an Analysis of the Storm and Flash/Sprite Developments

Maja Tomicic[1], Serge Soula[2], Eric Defer[2], Serge Prieur[2], Janusz Mlynarczyk[3], Thomas Farges[4], Olivier Chanrion[1], Christoph Köhn[1]and Torsten Neubert[1]

[1]DTU Space, Technical University of Denmark, Lyngby, Denmark
[2]Laboratoire d'Aérologie, Université de Toulouse, UT3, CNRS, IRD, Toulouse, France
[3]Department of Electronics, AGH University of Science and Technology, Krakow, Poland
[4]CEA, DAM, DIF, F-91297, Arpajon, France

Key Points:

- A high percentage (90%) of dancing sprites were produced by a large asymmetric MCS which developed in strong convective conditions over the Mediterranean Sea
- The sprite parent flashes mainly initiated at the edge of the convective region and propagated 100-200 km across the stratiform region
- An especially bright and wide sprite sequence was produced by three distinct positive CG strokes that occurred within 3 ms and were separated by 54 km

Corresponding author: Maja Tomicic, majtom@space.dtu.dk

Abstract

One of the most enigmatic types of sprites is the dancing sprite which appears to dance above the storm as sequential luminous emissions a few 100 ms or less apart. Dancing sprites occur in relatively small proportion and many aspects of their generation remain unknown. We present a multi-instrumental analysis of a 20-hour duration Mesoscale Convective System (MCS) over the northwestern Mediterranean Sea on September 21, 2019, that produced 21 sprites recorded with a video camera, of which 19 (90%) were dancing sprites. The asymmetric trailing stratiform MCS developed in strong convective conditions having a CAPE of 3,500 J kg^{-1}. It formed several convective cores (up to 2,900 km^2 with cloud top temperature < -66°C) and exhibited a bow echo structure during the sprite production period. Using Lightning Mapping Array data, we show that the sprite producing positive cloud-to-ground (SP+CG) flashes mainly initiated at the edge of the convective line on the side of the stratiform region. The flashes propagated 100-200 km across it, producing both positive and negative CG strokes. The 19 dancing sprite events included 49 sequences, of which 46 were associated with distinct SP+CG strokes and 3 with surges during the continuing current. An especially bright and wide sprite sequence was produced by three distinct SP+CG strokes that occurred within 3 ms and spread over 54 km. This sprite sequence could be classified as a new sprite category resembling a "wall" but structured in three groups, each associated with one of the +CG strokes.

Plain Language Summary

One of the most enigmatic types of sprites is the dancing sprite which appears to dance above the storm as sequential luminous emissions a few 100 ms or less apart. Dancing sprites occur in relatively small proportion and many aspects of their generation remain unknown. We present a multi-instrumental analysis of a 20-hour duration Mesoscale Convective System over the Mediterranean Sea on September 21, 2019, that produced 21 sprites, of which 19 were dancing. The storm developed in strong convective conditions and formed several convective cores with very high clouds and a bow-echo structure. Most of the sprite producing flashes propagated from the convective to the stratiform region over long distances producing strokes of both polarity. The 19 events included 49 sprite sequences, of which 46 were associated with distinct strokes and 3 with surges during the continuing current. An especially bright and wide sprite was produced by three strokes that occurred within 3 ms and separated by 54 km. This sprite could be classified as a new sprite category resembling a "wall". We accredit the high proportion of dancing sprites to a complex charge structure in the stratiform region with large potential and pockets of charge driving the leaders and allowing substantial discharge.

1 Introduction

Sprites are brief optical emissions occurring in the mesosphere above a thunderstorm as shown by low-light cameras (Sentman et al., 1995; Lyons, 1996). The phenomenon is triggered most often by a positive cloud-to-ground lightning stroke (+CG) that lowers a large amount of positive charge to the ground and exhibits a high charge moment change (CMC) (Pasko et al., 1997). Sprites can extend over an altitude range from 40 to 90 km and span 50-100 km horizontally (e.g Pasko et al., 1997; Neubert et al., 2008). The sprite discharge develops as positive downward streamers (cold plasma channels with enhanced electric fields in their tips), when the transient electric field exceeds the dielectric breakdown threshold at ∼70 km altitude (Pasko et al., 1997). High-speed camera observations have shown complex streamer propagation that induces various vertically structured shapes, both individually or in the form of sprite clusters (e.g Stanley et al., 1999; McHarg et al., 2007; Stenbaek-Nielsen & McHarg, 2008). Sprites are usually classified according to their optically perceptible characteristics as column, carrot, angel, wishbone, tree, jellyfish or combination of several of them (Bór, 2013).

Among the various types within the family of sprites, the dancing sprites constitute the longest lasting events. They consist of sequential luminous discharges visible at different locations above the storm over a duration of a few hundreds of milliseconds up to around one second. They are called dancing or jumping sprites and can extend over large distances up to more than 100 km (Lyons, 1994; Winckler et al., 1996; Lu et al., 2013; Yang et al., 2015; Soula et al., 2017; Bór et al., 2018). Such sprite events are observed in a relatively small number during a storm. For example, Bór (2013) made a statistical study over 489 sprite events of which only 44 (9%) could be classified as dancing. In some sprite producing storms, no dancing sprites are identified as in Soula et al. (2015) with 12 sprite events produced by a short lifetime storm. Lu et al. (2013) analyzed a total of 39 sprite events produced by a Mesoscale Convective System (MCS) near Oklahoma on June 29th, 2011, of which 14 were classified as dancing. In Lu et al. (2013) the dancing sprites were associated with a single lightning flash, but with three different schemes: the first where the dancing sequences could have been produced by distinct strokes of the flash, the second where they were associated with a series of current surges superposed on an intense continuing current, and the third was a mix of both. Soula et al. (2017) made similar observations for two cases of dancing sprites analyzed in detail. These included 4 and 3 sequences associated with sprite-producing +CG (SP+CG) strokes, and delayed sprite sequences or elements, clearly associated with surges of current. Bór et al. (2018) suggested that extended lightning flashes associated with large charge layers in the stratiform region are necessary for this kind of sprite event to occur.

The present study is a new analysis of a long duration storm (∼ 20 hours) that produced 21 sprites recorded during the night with a video camera, of which a very large proportion (90 %) were of dancing type. It is a combination of an overall presentation of the main characteristics of the dancing sprites, their production mechanism in terms of lightning activity and cloud structure, as well as a detailed analysis of three particular cases of these dancing sprite events. The paper is structured as follows: Section 2 describes the data and methods that were used in the study. Section 3 is a presentation of the storm that caused the dancing sprites. Section 4 is a general analysis/statistical study on the dancing sprites and their parent lightning. Section 5 presents the in depth analysis of three dancing sprite events. Finally, Section 6 discusses and summarizes the main results.

2 Data, instrumentation and methods

2.1 Optical observations

The sprite videos used in this study are provided in the Supplementary Information. They were recorded with a camera installed at the instrumental site of the Aerol-

ogy Laboratory (Laero): Atmospheric Research Center (CRA), in Lannemezan (43.127°N; 0.369°E; 600 m altitude). The camera is a Watec 902H with a field of view (FOV) of 31°, which is the same as described in Soula et al. (2017). The videos have a frame rate of 25 frames per second, or 50 interlaced fields per second corresponding to a time resolution of 20 ms. The beginning and the end of each video field is GPS time referenced (UTC time).

Since the sprites were only recorded by one camera, the triangulation of their geolocation was not possible, but their line of sight (LOS) from the camera location was computed. These LOS are based on the azimuth angles of the sprites in the video determined manually with the software "Cartes du Ciel" (SkyCharts) by matching visible stars in the images with the software star catalogue, given the observation time, the camera location and FOV.

In this work we adopt the classification and definition from Soula et al. (2017). A sprite event is defined as one video (of $\sim$ 2 sec duration) including one or more sprite sequences and a sprite sequence includes all successive video fields with sprite elements that appear as a consequence of one SP+CG stroke. In cases where the parent lightning stroke is not detected and since the relaxation time of the vertical electric field component above 60 km is less than 20 ms (Pasko et al., 1997), a sequence can be defined by sprite elements being separated in time by at least one field (20 ms).

According to the time interval with which they occur after the SP+CG stroke, sprites are usually classified as either long delayed (>20 ms) or short delayed (<20 ms), each exhibiting different characteristics in terms of SP+CG properties, displacement from SP+CG stroke and sprite morphology (e.g. Lu et al., 2013). For instance, Lu et al. (2013) showed that short time-delayed sprites had lower horizontal displacements from their parent +CG stroke. In this study we also classify the sprites based on the time delay from their parent SP+CG stroke. The delay is given as an interval because of the 20 ms time resolution of the videos.

2.2 Lightning data

The Vaisala Global Lightning Detection Network GLD360 (Said et al., 2010; Said & Murphy, 2016) is used to analyze the overall lightning activity produced by the storm. The data contain time, location, peak current and type (CG or IC) for each detected event. In Said and Murphy (2016) the detection efficiency (DE) of the network in the US is evaluated and they find a CG flash DE of $\sim$75–85% relative to the National Lightning Detection Network (which has a flash DE >95% (Mallick et al., 2014)). The DE over Corsica is assumed to be the same, because the sensor density in that region is similar to that in the US (R. Said, personal communication, March 17, 2021). We cluster the events detected by GLD360 (strokes for CG and pulses for IC) into flashes using the criteria that events within 20 km and 0.5 s of each other belong to the same flash. If one of the events in the cluster is identified as a CG, the flash is labelled as CG. The highest absolute value of peak current in the cluster is saved as the flash peak current and defines its polarity. If a flash is categorized as a CG flash but has a lower peak current than 5 kA, we assume that it is, in fact, an IC flash (R. Said, personal communication, May 7, 2020).

Lightning data from Météorage (MTRG from now) is used for the SP+CG strokes identification, in a complementary way to GLD data. It consists of time, location, peak current and stroke/pulse classification for CG strokes and IC pulses. The main characteristics of this network in terms of detection performances are described in Schulz et al. (2016) and Pedeboy (2015) and are valid at the date of the present storm. Schulz et al. (2016) showed that in a large part of France, the DE was 89% and 84% for negative and positive CG strokes, respectively. However, they show that the larger peak current values of the strokes the larger DE, suggesting a higher detection of SP+CG strokes that

generally exhibit rather large peak currents (São Sabbas et al., 2003; Lyons et al., 2003; Soula et al., 2009). The other important parameter for the study is the location accuracy (LA) of the SP+CG strokes. Pedeboy (2015) showed that LA was better than 120 m for 50 % of the strokes in the last two years of his study (2013-2014).

2.3 LMA

The development of the flashes and their 3D extension inside the cloud were mapped by the SAETTA Lightning Mapping Array (LMA) (developed by New Mexico Tech, USA (Thomas et al., 2004)) located in Corsica (Coquillat et al., 2019). The SAETTA LMA consists of 12 ground-based stations deployed evenly over the island and has a range of about 350 km centered on Corsica with good 3D mapping in a range of about 120 km. Each station measures the very high frequency (VHF) pulses produced by the leader phase of lightning flashes in the 60–66 MHz band. The LMA can locate the individual VHF sources in 3D by accurately measuring the time of arrival (TOA) of the signals with the use of GPS receivers with a theoretical location accuracy of about 200 m in the region where the studied TLEs occurred (Coquillat et al., 2019). For most SP+CG flashes only VHF sources detected by at least seven stations were used in the analysis (for the two last SP+CG flashes the criteria was lowered to six stations, because of poor reconstruction), and chi-squared goodness of fit statistics were required to be ≤ 0.5 in the source location solutions. These criteria minimize the influence of noisy or poorly located sources.

We analyzed the SAETTA data using typical 3D projections (e.g. Coquillat et al., 2019) (including movies), the time-distance plot (van der Velde & Montanyà, 2013) and also looked at the raw SAETTA data to identify regions with strong VHF radiation but poor reconstruction. Two approaches have been applied to identify all VHF sources that belong to a given flash. The first one relies on the analysis by visual inspection of the LMA data through a thorough analysis of multiple zooms, animations and interpolations of the propagation of the different components of a given flash. This was possible because of the limited number of cases to study and was also required because of the rather long range of the flash locations relative to the LMA center. A second approach was applied using the SAETTA source-to-flash algorithm, using a Density-Based Spatial Clustering of Applications with Noise (DBSCAN) method similarly to Fuchs et al. (2016) or Ma et al. (2021). Overall, by studying each of the 21 flashes, we concluded that the hand selection performs better than the automatic DBSCAN algorithm, which in the present case splits extended flashes because of a rather low density of the VHF sources at distant locations from the LMA center.

2.4 Extremely low frequency recordings

The continuing current is an important driver for triggering delayed sprites and of maintaining the quasi-static electric field in the mesosphere and thereby the sprite luminosity for longer than the local relaxation time (Pasko et al., 1997; Cummer & Füllekrug, 2001; Li et al., 2008; Lu et al., 2013; Soula et al., 2017; Bór et al., 2018; Gomez Kuri et al., 2021). The current moment waveform (CMW) and CMC for the SP+CG flashes were reconstructed from the data recorded by a broadband ELF measurement system located in the Bieszczady Mountains in Poland ($\sim$ 1500 km from the storm). It measures the magnetic field component of the electromagnetic field using two magnetic antennas, aligned in the north-south and east-west directions. They cover the frequency range 0.02 Hz to 1.1 kHz. The receiver features a Bessel anti-aliasing filter that has the energy bandwidth of 900 Hz. The sampling frequency is equal to 3 kHz. The CMW and the CMC were reconstructed using the method presented by Mlynarczyk et al. (2015). The method allows us to obtain the discharge parameters at the source, taking into account that the attenuation and the propagation velocity in the ELF range depend on the frequency.

Optical observations of sprites are very well correlated to electromagnetic field radiation in the ELF (3-3000 Hz) band (e.g. Cummer et al., 1998). When a bright sprite occurs, two peaks can be observed in the ELF signal, one due to the SP+CG stroke and a second one due to the current flow in the sprite. The delay between the SP+CG stroke and sprite as well as the sprite duration is therefore also seen in the ELF signal for these sprites (Cummer et al., 1998; Li et al., 2008). The reasons that only the brightest sprite events are seen in the ELF signal are not well understood (Cummer, 2003; Inan et al., 2010).

The vertical electric field was measured with a broadband vertical dipole whip antenna installed in the center of France (station F1 in Figure 1 in Kolmašová et al. (2016) ∼700 km from the storm location). A detailed description of the instrumentation is given in Farges and Blanc (2011). The frequency range of the antenna is <1kHz - 5 MHz and data are only acquired when the signal locally exceeds a threshold corresponding to an electric field amplitude of 2 V/m. When triggered, 30 ms of data with 6 ms of pre-triggering time at a sampling frequency of 12.5 MHz, are saved.

The electric field waveforms studied herein were all filtered with a digital low pass filter at 2 kHz. The ELF band is chosen because this is the range where we expect to see the sprite signature and it thus eases the interpretation of the data. However, it also eliminates any information about the currents on time scales shorter than 0.5 ms. Since studying the dynamics of the current flowing inside the lightning stroke and the sprite are outside the scope of this work and sprites usually appear at least 1 ms after the parent lightning stroke, this shorter time scale information is not important. When interpreting the filtered waveforms, one should be aware of artifacts introduced by the filter itself, which would appear as a 2 kHz signal in this case.

2.5 Cloud top temperature

The cloud structure and characteristics are evaluated from the cloud top temperatures (CTT) provided by the Meteosat Second Generation (MSG) Spinning Enhanced Visible and InfraRed Imager (SEVIRI) radiometer. The temperature accuracy is generally better than ∼1 K, the spatial resolution is 0.041° and every point in the observed hemisphere is observed four times per hour. The parallax error at this latitude (42.5°) is estimated to be about 14 km in north direction for cloud tops at ∼12 km altitude. All SEVIRI measurements analyzed here are corrected for parallax. By design, SEVIRI samples the geographical domain where the studied storm occurred at 11, 26, 41 and 56 min of each hour.

3 Overview of the storm structure and development

The dancing sprites analyzed in this study were observed on September 21, 2019, above a long duration (∼ 20 hours) MCS over the northwestern Mediterranean Sea. On this day, an east to south-east flow over the Mediterranean Sea, due to high pressure over Central and South Europe, carried hot and very humid air to South Eastern France at a lower level. This created convergence with the south-southwest cyclonic flow caused by a deep low of pressure located over the North Atlantic (980 hPa). It is in this context that the MCS developed early in the morning close to the Mediterranean Spanish north-east coastline and traveled east during the day, to reach Corsica at the end of the day. Figure 1 shows the motion of the CG lightning activity as reported by GLD360 during the entire life cycle of the storm. The storm trajectory above the Mediterranean Sea and the duration resembles that of the storm in Soula et al. (2017) that produced a large number of sprites, including dancing sprites.

In this study we focus on the afternoon and evening part of this storm, from 17:10 to 23:40 UTC. The CG flashes from this part of the storm are plotted in the zoomed inset in Figure 1 and the CTT development is displayed in Figure 2. This storm was a large

MCS covering more than 140,000 km^2 at its maximum (defined as the area with CTT < -40° C as inferred from CTT pattern issued from SEVIRI and referred to as A(-40°)), with the typical structure of a trailing stratiform MCS (Houze et al., 1990). A new storm started forming at 20:30 UTC east of Corsica, and the CG flashes from it are also plotted in the main part of Figure 1. The activity of the new storm is excluded from the analysis, as shown in the zoomed inset of Figure 1 where the CG flashes from it are not plotted.

The first sprite of the recorded period occurred at 18:39 UTC and the last one at 23:04 UTC and this is approximately the time period that we refer to as the sprite producing part of the storm. Figure 2 shows that the main cold/convective region (CTT<-65 °C) of the storm moved in a northeast direction during the sprite producing part of the storm and that the less cold/stratiform region (CTT>-60°C) was developed to the west and north. Also, it shows that most SP+CG flashes initiated close to or in the convective regions and the SP+CG strokes occurred in the trailing stratiform region. From Figure 2 we see hourly snapshots of the CTT, and the clouds could have developed or moved significantly at the time of the SP+CG relative to what is plotted here. The maximum value of this time difference is ∼24 minutes, which is for the last sprite event at 23:04 UTC.

The temporal evolution of CTT development and CG flash activity is shown in Figure 3. In the first hour (between 17:10 and 18:10 UTC), which corresponds to the beginning of the night for the region and is before the first sprite records, the storm was already well developed in size, but there had been a break in strong convection of a few hours. The convection started to increase around 17:25 UTC as seen from the area of cloud top with a temperature <-66° C (A(-66°) in Figure 3a) and was associated with an increase in CG flash rate and decrease in minimum CTT. The consistent observations are explained by the presence of updrafts that enhanced both the cloud electrification processes and the vertical development of the cloud. The lightning activity was highest from around 17:30 UTC to 19:30 UTC with a first maximum CG flash rate of 30-35 flashes per minute (fl min^{-1}) around 18:10 UTC. During this time, there were fluctuations in convection characterized by concurrent changes in A(-40°), A(-66°) and CG flash rate because of several convective cores that were successively more active. The two first sprite events happened during an increase in +CG flash rate between 18:30 and 19:00 UTC. After the two events and until 19:30 UTC strong convection intensified with minimum CTT of -73° C and CG flash rates above 30 fl min^{-1}. During this half hour period there were several high peak current +CG flashes but no sprite was recorded. From 19:30 UTC the CG flash rate decreased (especially for -CG) but A(-66°) increased in size and revealed from the CTT patterns in Figure 2 several small convective cells seemed to merge and became nearly circular until A(-66°) (blue regions in Figure 2 and pink bars in Figure 3a) reached the maximum size around 20:30 UTC, the same time as the high sprite rate began. The dissipating stage of the MCS was spread over time, with convective cores losing intensity one after the other. The minimum CTT started to increase from around 19:40 UTC and from around 20:30 UTC decreasing updrafts are also inferred based on reduced A(-66°) and CG flash rates. Most sprites were recorded between 20:00 and 21:00 UTC during the mature/dissipating stage of the storm and the sprite activity continued until the storm completely dissipated.

Whereas there is no obvious trend in the temporal development of the CG flash peak currents (Figure 3b), it is interesting to note that there were many strong +CG flashes that did not produce sprites within the FOV of the camera. Overall, during this part of the storm (from 17:10 to 23:40 UTC) 23 % of the CG flashes detected by GLD360 were of positive polarity.

4 Overview and analysis of sprites and parent flashes

During the night period of September 21, 2019, 21 sprite events were captured by the video camera, of which the location and FOV are indicated in Figure 1, 500-600 km away from the storm. These sprite events included from 1 to 4 sprite sequences, for a total of 51 sequences. In this work, the sprite events are numbered from 1-21 in chronological order. The histogram in Figure 4a shows the distribution of the number of sequences of the sprite events. It is interesting to note that only two of these sprite events exhibited one sequence, including the last event of the evening, which was a very bright jellyfish sprite. All other events (19 including 49 sequences) were dancing sprites (defined by at least two sprite sequences showing distinct separation in space or in time or in both), most of them with two or three sequences caused by individual SP+CG strokes from the same flash. Based on the analysis of VHF data described in section 2.3 all cases of dancing sprite events in this study were caused by continuous lightning discharge process and the sprites location followed the lightning propagation, something that was previously assumed by e.g. Soula et al. (2017); Bór et al. (2018) and is also shown by Lu et al. (2013) for several cases of dancing sprites.

In 42 out of 49 (87.75%) dancing sprite sequences, the sprites were produced by distinct +CG strokes separated in the flash; in the remaining 7 sequences no SP+CG stroke appeared immediately prior to the sprite. Data from GLD360 and MTRG were checked for positive and negative CG strokes that could be related to the sprite. When no SP+CG stroke appears, it could mean that a CG stroke was missed by the detection systems because the waveform of the VLF/LF signal was too complex or that the sprite was initiated by IC discharges or by intermittent surges during a phase with continuing current (van der Velde et al., 2006; Lu et al., 2013).

Figures 4b,c show the distribution of time and distance between the successive SP+CG strokes in a same sprite event (this could be determined when two successive SP+CG strokes were both identified, which was the case for 24 SP+CGs). The time ranged between 40 and 516 ms, with 80% being below 300 ms and the distance ranged between 2 and 87 km, which is in line with other studies of dancing sprites. In Lu et al. (2013) time intervals between successive SP+CG strokes within an event were in the range of 200-700 ms and the distances were in the range of 35-70 km. Bór et al. (2018) found time intervals of 48-277 ms and distances between 4.5 and 81.3 km. In Soula et al. (2017) the maximum distance between the first and last SP+CG stroke in one flash was $\sim$ 180 km and the time between successive SP+CG strokes was in the range of 270-700 ms.

Figure 5a shows the duration and horizontal extent of the sprite producing flashes for all events. The duration is defined as the time from the first detected VHF source to the last detected VHF source from the flash. The horizontal extent is defined as the maximum distance between two VHF sources belonging to the flash and is not necessarily the distance from the flash origin to flash termination. Care was taken to ensure that noise sources were not included in this calculation in two ways. First, noise sources were already removed in the initial filtering of the LMA data, and second, by visual inspection through plots of all sources from a given SP+CG flash with the ones used for the calculation highlighted. The horizontal extent of the sprite producing flashes ranges from 101 to 218 km and the parent flashes last from 1.3 to 6 s, most of them enduring between 2 and 4 seconds. Figure 5a also shows the time between flash initiation (first VHF source) to the first and last SP+CG stroke (when identified). Most of the flashes are seen to have continued after the sprite sequences, which usually occurred approximately halfway through the flash duration. Parent flashes of events #3 and #21 that only triggered a single sprite do not differ significantly from the dancing sprite flashes in these parameters.

Figure 5b,c summarizes the cloud characteristics where the 21 parent flashes propagated. Each event/flash has the number of sprite sequences annotated in Figure 5b, which also shows (in blue dots) $\Delta\mathrm{CTT}_{\mathrm{OT}}$ defined as the CTT difference of the the region of

flash initiation (± 0.05° in longitude and latitude of the mean location of the first 10 ms of VHF sources) and the same for the region of the VHF source furthest away from the initiation. Thus, a negative value means that the CTT around the flash origin was colder than the CTT at flash termination, meaning higher cloud top height at the flash origin. Since all values are negative, all SP+CG flashes initiated in colder regions than where they terminated. The orange dots are ΔCTT_{MO} and show the difference in CTT between the minimum CTT at the time of the flash and the CTT at flash origin. This suggests that most SP+CG flashes were not initiated within the coldest cores but they were initiated close to other convective cores in decaying phase. This behavior matches the initiation and stroke location of the SP+CG flashes seen in Figure 2. Figure 5b also shows the time from the SEVIRI scan until the event, referred to as Δt_{SF}. The maximum possible time is 450 seconds (7.5 minutes) meaning that the event occurred halfway between two scans. Accordingly, a time of zero seconds means that the event happened just as SEVIRI was scanning the region. Larger times indicate larger possible errors in the determination of CTT at specific parts of the flash, because the storm dynamics are relevant in 5-10 minutes timescales.

Figure 5c shows the mean VHF source altitude of the first 10 ms of the flash and the sources recorded during the sprite sequences (± 100 ms around sprites). The latter essentially provides an estimate of the positive charge layer altitude in the stratiform region where negative leaders propagate with a strong VHF signal (Shao & Krehbiel, 1996; Rison et al., 1999; Thomas et al., 2001; Lang et al., 2004). It shows that the flashes originated at various altitudes consistent with the findings by Lang et al. (2004) that stratiform +CG flashes originate at same altitude as other flashes. It should be noted, that in some cases the initial breakdown might not be reconstructed in the LMA data, and this might be just the early part of the flash rather than the actual initiation. On the other hand, the mean altitude of VHF sources recorded during the sprite events was between 6-8 km altitude for all of the first 14 events. From event #10, which was at 20:51 UTC, the altitude decreased slowly and continuously until it reached 4-5 km for the final events of the storm. This could indicate that the main positive charge region is located at ∼7 km altitude (typical charge removal altitude as seen by e.g. Lu et al. (2013); Lang et al. (2010)) from around 18-21 UTC and gradually drops to 4-5 km for the final stage of the storm. This pattern is also seen in Lu et al. (2013) and could be related to the weakening of the strong convection that happens around 21 UTC if it is assumed that charge advection from the convective regions is the primary source of charging for the layer at 6-8 km and this therefore only gets replenished while convection is strong (Carey et al., 2005; Lang et al., 2010). In addition, the combination of weaker updrafts and the carrying of positive charges by the precipitation will cause a net descent of the positive charge layer.

From the combination of the flash development parameters presented in Figure 5a-c, a common SP+CG flash propagation is observed. The fact that the leader processes initiated at varying altitudes and CTT values suggest that there was not a specific region in the storm that was responsible for SP+CG flash initiation. However, according to ΔCTT_{OT} (Figures 2 and 5b) the SP+CG flashes initiated close to the convective regions and travelled to the stratiform region more than 100 km from the origin predominantly in a direction pointed away from the convective regions and the storm direction. The VHF altitude during the sprite sequences, which occurred approximately halfway through the flash duration, was constant around 6-8 km for the most of the sprite period but descended to 4-5 km from the time when strong convection ceases. The flash behaviour is very similar to the one described by Soula et al. (2017) and similar flash propagation is also reported in Lu et al. (2013); Lang et al. (2010); van der Velde, Montanyà, et al. (2010).

5 Dancing sprite cases

The following section presents three case studies of dancing sprites. The dancing sprite events are chosen because they represent typical events from the storm and include interesting flash behavior.

5.1 Event 6 at 20:30:52 UTC

This event is a dancing sprite with three sequences that occurred during the most sprite producing period of the storm. The parent flash was a complex flash that produced 21 IC pulses and 18 CG strokes detected by MTRG within a duration of 2.15 seconds. Strokes and pulses that were detected twice by MTRG were only counted as one in the values given here. The characteristics of the SP+CG strokes, as well as the sprite delay (Δt sprite), are listed in Table 1. In Figure 6a we show the brightest video field for each sequence and Figure 6b shows the altitude of the VHF sources with time. The first sequence (sprite 6a) occurred between 20:30:52.569 and 20:30:52.589 UTC as seen from the timestamp in the bottom of the first video field. It followed two +CG strokes (63 kA and 35 kA, respectively) both of which initiated continuing currents as seen from the CMW plotted in Figure 6b. Sprite 6a was produced with short delay after the second +CG stroke that gave rise to a current surge superposed on the continuing current from the first stroke that had not settled yet. The same mechanism is also observed in event 26 reported by Lu et al. (2013). The sequence is visible in one to two fields, before another sequence (sprite 6b) appears. Sprite sequence 6b seems continuous from sequence 6a, but at an azimuth further south. Sprite 6b is visible in nine consecutive fields (corresponding to <180 ms) corresponding to the persistence of the continuing current initiated by the second +CG stroke. The CMW (Figure 6b) and the electric field waveform (the second panel of 6e) show that the first +63 kA stroke has only one peak related to it while the +35 kA stroke that triggered sprites 6a and 6b looks like two strokes 5 ms apart. No other discharge was located at this time by VLF/LF lightning detection systems (the next detection was an IC pulse after 12 ms), and while two strokes that are close together can be reported as one because the two signals mix, this is unlikely at a 5 ms time difference. Based on the timing of the pulses, the lack of other detections and the $\sim$ 5 ms duration of the second pulse we speculate if it could be caused by sprite 6a, even though it was not very bright. Otherwise, the second pulse could be a stroke that was missed by MTRG and GLD360 and could be the triggering stroke for sprite sequence 6b. The total CMC including the stroke and the continuing current with surges over 180 ms was 3432 C km. The two +CG strokes discussed so far occurred close to the main cold CTT region (see Figure 6d) but following them the negative leader was accelerated and escaped into the stratiform at high speed ($\sim 10^6$ m s^{-1}) as seen in the time-distance graph (Figure 6c) around 0.75 s. During the fast expansion and branching of the leaders in the stratiform region the density of VHF sources is low, but we see that they reached a distance of $\sim$100 km before an exceptionally bright sprite cluster appeared (sprite 6c) and was visible in one field (< 20 ms). This sprite resembles a wall and spanned 6°35' in azimuth corresponding to around 65 km at 550 km distance from the camera.

Sprite 6c occurred with a short delay after three strokes, see Figures 6b-e and Table 1. First, two +CG strokes of 42 kA (to the north) and 14 kA (to the south) were detected, separated in time by 1 ms but 54 km apart. 2.5 ms after these two strokes a +CG stroke of amplitude 78 kA was detected approximately in the middle between the two previous strokes. All strokes resembled the leader development scenario "negative leader cutoff" explained by van der Velde et al. (2014) because they occurred far inside the stratiform region close to a fast negative leader. The low number of VHF sources prior to the strokes can be explained by substantial branching of leaders. This would mean that the strokes were triggered from separate leaders, which is also indicated by the positioning of the strokes relative to each other. It is interesting to note that the two earlier +CG strokes (42 kA and 14 kA) spanned almost the whole extent of the 60 km wide sprite,

Table 1. SP+CG strokes for event #6 at 20:30:52 UTC. The first column indicates the sprite sequences (a, b, or c).

Sprite	Time *	Lon [deg]	Lat [deg]	Peak current [kA]	CMC [C km]	Δt sprite [ms]
a / b	52.485	7.52	42.90	63	770	-
a / b	52.574	7.40	42.81	35	3432	0-15 / 15-35
c	52.887	6.81	42.67	42	4295**	-
c	52.888	6.39	42.30	14	4295**	-
c	52.890	6.57	42.51	78	4295**	0-19

*seconds after 20:30.
**cumulative CMC for three last strokes.

thus, the sequence of three +CG strokes could explain the exceptional brightness and the width of sprite sequence 6c. The unusual SP+CG stroke series preceding this sprite sequence will be discussed in more detail in section 6.

The electric field waveform for sequence 6c is shown in Figure 6e and reveals three peaks. The first two peaks are 2.5 ms apart, like the time difference between the first two strokes and the last one. Also, the second peak has a higher amplitude, just like the stroke currents. Following them, with a few ms delay, is a pulse of $\sim$ 5 ms duration probably caused by the bright sprite. In the CMW shown in 6b all three peaks are merged because of the time resolution of the equipment but the amplitude is 606 kA km, which is four times higher than for the two previous +CG strokes (both of $\sim$ 150 kA km), and the total CMC was 4295 C km. After the sprites, the density of VHF sources increased and most of them are seen as negative leaders that propagated in the stratiform region at an altitude of $\sim$ 7-9 km.

5.2 Event 9 at 20:38:38 UTC

This dancing sprite includes 4 sequences produced through distinct strokes. The event clearly followed the flash path as seen from VHF sources and the four sequences were short, at about constant time interval (around 200 ms) and coincided with the SP+CG strokes (see Figure 7). The flash originates at an altitude of 2-3 km northwest of the coldest CTT region. Although the VHF sources in Figure 7b,d only show a few sources at the location of flash initiation, we have verified that this is most likely the flash origin in the raw SAETTA data. The first sprite sequence is visible in three video fields and occurred with a 44-64 ms delay after a 63 kA +CG stroke. This stroke was the first discharge that was recorded by MTRG during the flash and based on the distance of 9 km from the flash origin (see Figure 7c), it could have been the positive leader from the initial breakdown that approached the ground. The stroke initiated a continuing current with two surges as seen in Figure 7b. The first is consistent with a current waveform due to M-components, furthermore the timing matches an IC discharge after $\sim$ 60 ms and the second is consistent with a +CG stroke (of peak current 27 kA) after $\sim$ 180 ms. The timing of the first current pulse matches the time that the sprite appears in the video, thus the current surge from M-components or from the recorded IC pulse could be the trigger for sprite sequence 9a. In addition to creating a continuing current and stress above the cloud, the first +CG stroke also initiated new breakdown and negative leaders propagated from the area discharged by the +CG stroke. After the +CG stroke the flash developed two major extensions as evident from Figure 7d. One was very well detected with many sources and ascended from 4 km to 10 km while propagating in a circular path towards the convective core, where it stopped. The other part of the flash propagated to-

wards the southwest and into the stratiform region, where it developed several branches and triggered three more sprite sequences.

Table 2. SP+CG strokes for event #9 at 20:38:38 UTC. The first column indicates the sprite sequences (a, b, c, or d).

Sprite	Time *	Lon [deg]	Lat [deg]	Peak current [kA]	CMC [C km]	Δt sprite [ms]
a	37.996	7.41	42.91	63	5590**	44-64
b	38.257	7.07	42.68	62	1029	3-23
c	38.523	6.34	42.46	65	906	0-18
d	38.703	6.98	42.32	102	1659	0-17

*seconds after 20:38
**cumulative CMC until SP+CG b.

Sprite sequence 9b appeared at a LOS a little more south of sequence 9a following the propagation of the VHF sources (Figure 7d). It is only visible in one field (<20 ms) and was a short delayed sprite caused by a CG stroke of similar peak current (62 kA measured by MTRG) but higher current moment than the previous. The last two sequences of this event were also short delayed and occurred further south in the direction of flash propagation. Sequence 9c is visible in three fields (<60 ms) and sequence 9d is visible in two fields (<40 ms). Table 2 and Figure 7 show that the latter was the brightest appearing sequence of this event and was caused by the strongest SP+CG stroke (102 kA). After the sprite sequences the leader travelled in a southeast direction in several branches with sources distributed in a layer of about 2 km width.

5.3 Event 17 at 21:48:09 UTC

Event 17 is a dancing sprite with three sprite sequences that occurred during the dissipating stage of the MCS. Figure 8a shows the brightest video field for each sequence. The flash lasted for 4.8 seconds, had a horizontal extent of 218 km, and MTRG reported 33 IC pulses and 19 CG strokes during the flash. Figure 8d shows that the flash originated close to the edge of the cloud near a convective region with CTT between -65°C and -70°C. As shown in Figure 3a at the time of this event, there was a decrease of the minimum CTT and a small increase of A(-66°) from 21:25 UTC for about one hour, which indicates a slight and local reactivation of the convective activity. At the time of the first sprite, the flash had already endured for over 3 seconds, but as seen from Figure 8c,d the leaders stayed close to the flash origin until around 400 ms before the sprite. At this time, the leaders ascended to 9-10 km altitude and just before the first SP+CG stroke a fast negative leader descended from ∼10 km to ∼6 km altitude and accelerated into the stratiform region. The first SP+CG stroke could be related to this sudden acceleration as explained by the 'Slow-fast bidirectional development' (van der Velde et al., 2014). Sprite 17a was a long delayed (25-45 ms) and long duration (7 video fields corresponding to <140 ms) sprite that appeared after a +27 kA +CG stroke (see Table 3 for all SP+CG strokes for this event). The duration of the sprite luminosity matches the continuing current from the stroke as seen from the CMW in Figure 8f. The stroke did not exceed the detection threshold at the location of the vertical whip antenna, which is why there is no electric field waveform plotted. The continuing current did not settle until the next SP+CG stroke occurred and the sprite luminosity is continuous between sprite sequences 17a and 17b. During the continuing current the VHF sources travelled at ∼ $3{\times}10^5$ m s^{-1} approx. 140 km away from flash origin until a 142 kA +CG stroke coming from the fast negative leader, probably by the mechanism of negative leader cutoff (van der Velde et al., 2014), caused sprite 17b. This was a short delayed, very bright sprite

and is only visible in one field. The electric field data in Figure 8e show a pulse synchronized with this SP+CG stroke and a second pulse 2 ms later. Since there were no CG strokes detected at this time and the sprite was very bright, the second pulse is likely to be caused by the sprite. As seen from the CMW in Figure 8a the current moment was almost 900 kA km and the total CMC was calculated to 3320 C km (this is a little underestimated because the integration starts from the continuing current of the previous sprite sequence).

Table 3. SP+CG strokes for event 17 at 21:48:11 UTC. The first column indicates the sprite sequences (a, b, or c).

Sprite	Time *	Lon [deg]	Lat [deg]	Peak current [kA]	CMC [C km]	Δt sprite [ms]
a	11.216	8.34	42.09	27	4000**	25-45
b	11.389	7.61	42.65	142	3320	0-12
c	11.470	7.31	42.79	51	1421***	-
c	11.471	7.46	43.06	44	1421***	-
c	11.471	7.38	42.91	62	1421***	0-10

*seconds after 21:48
** integration stopped at SP+CG 17b.
*** cumulative CMC for three last strokes.

Sprite 17c was a short delayed sprite and is visible in two video fields. It was preceded by three +CG strokes presented in Table 3. The CMW shows three strokes in a rapid sequence and the total CMC was 1421 C km. The production mechanism resembled that of sprite 6c, however, in this case the LOS to the sprite was displaced from the +CG strokes in a direction corresponding to the VHF source propagation. The ELF electric field waveform from sprite 17c shows two pulses separated by 1.2 ms. This corresponds to the time difference between the first and the two subsequent strokes.

6 Discussion and conclusions

6.1 Meteorological conditions

The sprite events captured during the night of 21st September are distributed over a little more than 4 hours between 18:39 and 23:05 UTC with a large proportion within a period of about 1 hour 40 min between 20:19 and 21:58 UTC. The proportion of dancing sprites is exceptionally high when comparing with published studies about this specific type of sprite event, especially with the statistical analysis over 489 sprite events by Bór (2013) where only 9 % were classified as dancing. Another case of a storm within the same area provided also several cases of dancing sprites, of which two were analyzed in detail by Soula et al. (2017). Revisiting the data of this case with more than 120 sprite events observed by a low light camera located at Pic du Midi (42.93°N; 0.14°E; 2877 m), the authors checked that more than 50 % of events could be considered as dancing sprites. Of course, the number of sprite events is considerably larger in Soula et al. (2017), especially because the storm activity lasted later during the night since the last event was detected at 05:32 UTC on 30th October 2013, while the first was detected at 17:49 UTC on 29th October 2013. Next to that, both storms (Storm 1 for Soula et al. (2017) and Storm 2 for the present storm) exhibit some similarities and differences: (i) Both have a very long lifetime of 18 hours (10:00 - 04:00) and 20 hours (04:00 - 24:00), for Storm 1 and Storm 2, respectively. Storm 1 activity started close to the coastline of Catalonia in Spain and Storm 2 started over northeastern Spain, then both moved to the east above the Mediterranean Sea during the day and a part of the night. (ii) For CG lightning ac-

tivity, both storms exhibit similar maximum CG flash rates around 30-35 fl min^{-1} just before the first sprite events were observed. (iii) In both storms, several convective cores are visible from the radar observation, which correspond to different cells producing several successive maxima of the CG flash rate. (iv) Both could be classified as an MCS at very close to the maximum size when the first sprite events were observed for Storm 1 or just before for Storm 2, with an area of 140,000 km^2 with a cloud top temperature colder than -40°C and a minimum CTT of -73°C. Furthermore, both storms exhibited a large area with cold cloud tops (colder than the tropopause, i.e. overshoots), around 6,000 km^2 with CTT below -65°C for Storm 1 and 2,900 km^2 with CTT below -66°C for Storm 2. This characteristic could favor the production of flashes with a long propagation distance that should be at the origin of dancing sprites. By looking at other cases of sprite-producing storms in the literature for which the cloud top temperature is analyzed (Soula et al., 2009, 2015) such large overshoots are not observed, even when the storm produced a very large amount of sprites (São Sabbas et al., 2010). To analyze the meteorological conditions, the Convective Available Potential Energy (CAPE) values are calculated for both days at 00:00 UTC. They are much larger for the present storm with about 3500 J kg^{-1} within a large area over Mediterranean Sea while it is only between 1500 J kg^{-1} and 2500 J kg^{-1} within the same area for Storm 1. The large values of CAPE lead to strong convection and large vertical development of the clouds. Assuming the parcel theory, the vertical velocity within the convective clouds is linked to the CAPE (Jacobson, 2005):

$$W = (2 \times CAPE)^{1/2} \quad (1)$$

In the present case, the tropopause temperature was -63°C in the region of the storm when sprites were produced according to the NCEP/NCAR reanalysis which shows high and large overshoots for this storm. Indeed, the minimum CTT was -73°C which was about 10°C colder than the tropopause. It corresponds to a height of 1 km above the tropopause, according to the adiabatic transformation temperature cooling rate (-9.8° km^{-1}), which can be considered at this altitude (Jacobson, 2005). Such persistent and large overshoots indicate a strong convection and the production of a large amount of charges. Ice crystals carry charge towards the upper part of the thundercloud. This charge (positive in a normal dipole/tripole charge structure) pushed out of the convective core by the strong permanent updrafts and advected towards the stratiform region, can contribute to the extended reservoir of charge for the SP+CG flashes (Lang et al., 2004; Carey et al., 2005; Lu et al., 2009; van der Velde et al., 2014). The wind shear is also analyzed for the day of the storm. Indeed, the vertical shear of the wind with strong winds at upper levels can help to explain the advection of the upper cloud charge in the stratiform region and an increase of the positive CG flash rate (Carey et al., 2005). This advection of the upper charges could also support the unbalanced main charge poles to explain the conditions favorable to trigger gigantic jets (van der Velde, Bór, et al., 2010). Furthermore, the storm analyzed in van der Velde, Bór, et al. (2010) was exactly at the same location as the present storm when the sprites were produced. The authors reported a wind shear of 35 m s^{-1} between 0 and 6 km. In the present case, we observe a rather large shear in wind velocity, and less in wind direction. The wind was northward/northeastward and strong at the upper levels (up to 30 m s^{-1} at 300 hPa level which was also the altitude of the maximum (eastward) wind velocity in van der Velde, Bór, et al. (2010)). At lower level we obtain weaker winds (around 10 m s^{-1} at 900 hPa level, according to the location). Thus, we can consider a maximum wind shear of about 20 m s^{-1} between the levels 900 hPa ($\sim$ 1 km) and 300 hPa ($\sim$ 9.2 km). This value is typical of the environmental conditions for the MCS developments, i.e. 15 m s^{-1} for the layer 0-6 km in Carey et al. (2005).

Other cases of storms producing sprites within the same area and already analyzed by some of the authors are also compared. It is the case of the storm during the HyMeX campaign on 22 October 2012 (Soula et al., 2015) which produced 11 sprite events but no dancing. In this case, the storm had a short lifetime (3-4 hours), a low maximum of CG flash rate (about 4 flashes min^{-1}), a minimum CTT of -62°C, and the CAPE was

about 1 kJ kg^{-1} within the region of the storm. Another storm produced very large sprites on the night of 01-02 September 2009 over the Mediterranean Sea (Soula et al., 2014). The number of sprites was low in this case, with only 9 events for one hour, but some were exceptionally bright and large. Three of these events could be considered as dancing, with at least two sequences associated with different positive strokes. The CG flash rate was very high for a short duration before the sprite production with about 45 CG flashes min^{-1} and the minimum CTT at that moment was -71°C. The size of the storm was also much smaller with only 70,000 km^2 and CTT < -35°C when the sprite events were produced. This storm seems to have had a feature of strong and rapid development followed by a fast collapse before the sprites. It developed over the Pyrénées range during the afternoon and then moved eastward during the evening by producing a moderate CG flash rate compared to that reached before the sprite events. The CAPE values were around 2 kJ kg^{-1} within the area of this storm. It shows the number and the type of sprite events are associated with the convective conditions in which the storm develops.

6.2 Analysis of the dancing sprite sequences

In our observations of several cases of dancing sprites we obtain different chronologies of sprite sequences and lightning flash processes. We classified 19 sprite events (out of 21) as dancing, which means we identify at least two sequences within them. It is a large sample to analyze different scenarios of this kind of event. First, we can address what is a sequence in a sprite cluster that looks like a dancing (or jumping) sprite, from observations with only one video camera. As indicated by Lu et al. (2013), dancing/jumping events associated with a single lightning flash could be produced either by distinct strokes of the flash, by a single stroke through a series of current surges superposed on an intense continuing current, or by both. We can therefore observe three kinds of subsequent sprite sequences that form dancing sprites: (1) those that occur with a discontinuity of luminosity from the previous one, with a time interval long enough to be seen like that by the 20 millisecond-resolution video camera (interval between two fields), with an apparent shift in space and associated with a new SP+CG stroke; (2) those that occur in a continuous light emission with elements that are spatially shifted from field to field; (3) those that occur with a discontinuity of luminosity but without displacement (or small displacement). Of course, both discontinuity and apparent displacement of the sprite elements depend on the camera time resolution and location relative to the sprite event, respectively.

According to the present number of dancing events (19), we have therefore at least 19 subsequent sequences. By looking at the video imagery of all these events and the stroke detection system data, we count 30 subsequent sequences, as indicated in Figure 5b. A large majority of these sequences correspond to type 1, probably at least 21 out of 30, with a small uncertainty according to the video imagery perception. Some examples from the case studies in section 5 corresponding to this type are sequences 9b, 9c, 9d or 17b. Four other sequences (5b, 14b, 18b and 20b) are largely displaced from the previous sequence (5a, 14a, 18a and 20a) and could be classified as type 1 by considering the SP+CG strokes were missed by the lightning locating systems. Some sequences correspond to type 2, insofar as they follow the previous sequence without any apparent break of luminosity but a large displacement over several fields as in sequences 6b (in section 5.1 and Figure 6), 7b and 7c. According to the analysis in section 5.1 this type of sequence of sprite elements should be produced during the continuing current following the previous stroke that produced a sequence of the sprite event. Indeed, the conditions of electric field at the triggering altitude for sprites (generally around 70 km) can be maintained by the charge flow during the continuing current and associated surges of current (M-components) as already noted by Lu et al. (2013) and Soula et al. (2017). The present sequence 6b illustrates very well the long duration of this type of sequence (9 fields from the video im-

agery, i.e. < 180 ms) and its shift from the initial SP+CG stroke that progresses above the stepped leader within the cloud, as indicated by Lu et al. (2013).

We have two more sequences, 6c and 17c, that are not associated with one SP+CG stroke but with three SP+CG strokes occurring within a very short time interval, 3 and 2 ms, respectively. In both cases, they are the last sequence of the event. Sequence 6c (presented in Figure 6) is an exceptionally bright and wide sprite sequence with a shape that resembles a curtain or a wall. Three +CG strokes were detected within 3 ms and about 5 ms prior to the sprite ELF signature shown in Figure 6e and as mentioned in section 5.1. The distance between the northern and southern strokes spanned over 54 km while the whole extent of the sprite in the FOV of the camera is around 65 km. We propose two mechanisms that could explain the relationship between the three +CG strokes and the sprite. (i) Potentially the sprite is a new type of sprite sequence within the dancing sprite category, namely one where the individual sprite sequences are triggered by strokes that are separated by only 3 ms (or less) and therefore are not resolvable in the video field due to its temporal resolution. The atypical morphological characteristics of the sprite sequence supports this explanation, since it would mean that it consists of three sprite sequences partly overlaid in the image and thus, the dancing appearance is not seen, even if the sprite sequences are triggered one after the other. (ii) On the other hand, the mechanism could be that the three +CG strokes discharge a very large region of the stratiform region prior to the sprite sequence. The multiple +CG strokes, within the relaxation time at sprite altitude, would enhance the transient electric field in three overlapping regions and thereby increase the volume of the upper atmospheric region where conditions necessary to initiate and propagate streamers exist allowing the horizontally extensive sprite sequence. By examining in detail the image of the sprite sequence (Figure 6a, zoom of sprite 6c) it is possible to distinguish three structures (defined in Figure 6a with white dashed frames), each with column elements on the edges and a bright structure in the center. The observation of large and luminous sprites shows typically this distribution of elements as for example in Soula et al. (2014), Fig. 5, or in Bór (2013), Fig. 8. Qin et al. (2013) shows theoretically that columniform sprites may also appear in the periphery of a sprite halo produced by +CG strokes associated with large CMC, while carrot sprite elements are produced centered below the halo. Actually, the columniform elements are produced in lower transient electric field. The sprite sequence 6c could support the first mechanism proposed.

Sprite sequence 17c is also preceded by three +CG strokes produced within 2 ms and with a delay < 10 ms (Table 3). The three strokes spanned over a distance of 32 km between the southern and the northern extent. As seen in Figure 8a sprite sequence 17c is not particularly bright, although it has a curious shape and two point-like elements are visible to the right of the main sprite elements. The main sprite element is shifted to the north relative to the strokes (Figure 8d). The point-like elements seem to be rebrightening of parts of the previous bright sprite sequence (Sequence 17b) and are well aligned with the line of sight of two out of the three strokes. For this case, the sprite elements are more faint and narrow, compared to those of Sequence 6c. A large difference is also observed for the cumulative CMC relative to the three strokes, 4295 C km for Sequence 6c and only 1421 C km for Sequence 17c. According to the shift of the main element, this case does not seem to correspond to mechanism (i) but rather to mechanism (ii) where the combination of the three strokes allows the sprite triggering in a given region of the mesosphere. Camera observations in higher temporal resolution or from multiple locations are necessary to confirm any of the two mechanisms.

6.3 Storm structure and SP+CG flash propagation

Figure 9a,b,e,f,i,j shows the reconstructed radar reflectivity at 2-3 km altitude and Figure 9c,d,g,h,k,l shows the horizontal and vertical extent of the VHF source density for three of the events in this storm (event #4 at 20:19:04 UTC in the top panel, event

#9 at 20:38:38 UTC in the middle and event #16 at 21:39:13 UTC in the lower panel). Overlaid in Figure 9 are the reconstructed VHF sources belonging to the respective SP+CG flashes. From the radar data in Figure 9a,b we see that at 20:20 UTC the storm exhibited a bow-echo structure in the convective line and at this time the overall storm structure can be classified as an asymmetrical bow-echo MCS, resembling the example of an asymmetric structure shown in Figure 9f in Houze et al. (1990) and the storm that was studied in detail in Lang and Rutledge (2008). The asymmetry is identified from the strongest convection being located in the southern portion of the MCS and the stratiform region being more developed to the north of this convection. When comparing with Figure 2 in the present study, it is seen that the CTT was colder right behind the bow-echo and in an elongated region to the north of it, which matches the regions of high radar reflectivity.

The convective charge structure is suggested by the VHF source density plots in Figure 9d,h,l for the time around the three sprite events (and around all sprite events in Figure S1 in the supplemental material). It appears to be complex and evolving rather rapidly in different charge configurations that do not allow to easily propose a specific 3D distribution. However, the strong maximum of VHF source density around 5 km altitude in the bow-echo (as seen from Figure 9d and 9h) allows us to infer that this region is favorable to the propagation of negative leaders, since they strongly radiate in VHF, and therefore corresponds with a positive charge layer. Furthermore, at the same time that the bow echo appears (around 19:30 UTC) the -CG flash rate decreases considerably as indicated in Figure 3a. This suggests that the charge structure in the bow-echo was an inverted dipole, which was also the case in Lang and Rutledge (2008). Sprites associated with an inverted charge structure were also observed by Lang et al. (2016) in a storm that also developed in strong CAPE conditions (> 2.6 kJ kg^{-1}) and large wind shear (15 m s^{-1} between 0-6 km). Although the majority of the electrical activity, probably associated with IC flashes, was in the bow-echo as seen from the VHF source density (Figure 9c), the majority of SP+CG flashes did not start in this part but close to small convective regions north of the bow-echo as the example in Figure 9b, where the star represents the flash origin. We attribute this to the stratiform region that is developed at the rear of this part of the convective leading line and allows the negative leaders to propagate within and towards positive charge layers. Furthermore, negative strokes are also detected in the stratiform region (Figures 6, 7, 8) which means negative charge layers are also present within this region. The stratiform charge regions can have two origins, either created by charging processes associated with mesoscale updrafts as explained by Dye and Bansemer (2019) or carried from the convective line by advection (Carey et al., 2005) or a combination. Advection of negative charge could occur when the charge structure in the convective line is inverted as proposed by Lang and Rutledge (2008). From the radar data (Figure 9) we also see some variations in the radar reflectivity ≥ 35 dBZ inside the stratiform region that have more structures than the typical secondary maximum of radar reflectivity as described in e.g. Braun and Houze (1994). These structures can support mesoscale updrafts as proposed by Dye and Bansemer (2019) who combined both in-situ electric field and microphysics measurements, by penetrating within the stratiform structures. They explain the presence of double polarity charge layers by non-inductive charging processes, that occur during non-riming collisions between ice particles in the absence of supercooled liquid water. Their observations showed large electric fields over large extents, highly stratified radar reflectivity lower than 30 dBZ and large non-riming aggregates. These combinations are indicators of mesoscale updrafts. In the present case, the reflectivity values observed (>35 dBZ) over large structures within the stratiform region could be explained with mesoscale updrafts. The propagation of the reconstructed VHF sources from the SP+CG flashes were often well aligned with these regions of higher radar reflectivity in the direction pointing away from the convective line (e.g. event #16 in Figure 9j). Some sprite-producing flashes were observed to trigger within this region at low altitude (event #9 in Figures 7 and 9f), to propagate up to about 8 km altitude and to produce CG strokes of both polarities. From here,

the leaders propagated in the direction towards the convective line, as they followed the same conduit observed in prior studies (e.g. Carey et al., 2005) but in the reverse sense. In addition, many SP+CG strokes occurred in these regions (see Figure 9a,e), implying that they were regions of charge concentration.

Thus, from the reconstructed VHF sources a rather common propagation of SP+CG flashes is observed. Most of them initiate in or close to the convective region and then escape far into the stratiform region with several ground connections of both polarities. This kind of flash propagation is also seen in e.g. Lang et al. (2004), van der Velde, Montanyà, et al. (2010), Soula et al. (2017). However, compared to similar studies, the SP+CG lightning flashes from this storm were longer both in terms of duration and horizontal extent. The average horizontal extent was 156 km with a standard deviation of 31 km and the average duration was 2.9 seconds with 1.3 second standard deviation. These values are 3-4 times higher than what is reported in van der Velde, Montanyà, et al. (2010) for sprite producing flashes in a small MCS in northeastern Spain and also higher than the +CG lightning flashes in Lang et al. (2004) which focuses on the stratiform +CG lightning from the storm in Lang and Rutledge (2008). Montanya et al. (2014) reported on 1047 flashes recorded by the Ebro delta LMA in Spain and said that the median flash length was 20 km and the median duration was 0.4 s. In comparison, the SP+CG flashes from this study could all be considered as extremely long. The long propagation of the flashes and many distributed +CG strokes might be necessary for the production of dancing sprites.

The long extent and duration of the flashes examined in this study match the criteria for the so-called 'negative leader cutoff' scenario described in e.g. Krehbiel (1981), Nag and Rakov (2012) and van der Velde et al. (2014). This is a +CG stroke (and sprite) production mechanism where a negative leader travels from the flash origin in the convective region far (tens of km) into the upper positive layer of the stratiform region. Here the leader is cut off because it is not able to sustain sufficient current. After the cut off new positive leaders start from the rear of the progressing negative leader producing a +CG stroke away from the flash origin, under the stratiform region. This scenario is suggested in VHF data by the positioning of a +CG stroke under a long-lasting negative channel in the stratiform region and by the absence of VHF sources/traces linking the +CG stroke to the flash origin. In the case studies presented in section 5, we see examples that resemble this mechanism: sprite 6c, 9b,c,d and 17b,c. However, we also see examples (e.g. sprite 6a,b sprite 9a and sprite 17a) where negative leaders abruptly accelerated into the stratiform region and the point from which they accelerated was accompanied by a +CG stroke. This resembles the mechanism 'Slow-fast bidirectional development' from van der Velde et al. (2014). A combination of these two mechanisms is common in the observed flashes primarily in such a way that negative leaders were accelerated from the convective regions to the stratiform region in a process that was accompanied with a +CG stroke and afterward the negative leaders were cut off as they propagated in the stratiform region resulting in new +CG strokes.

6.4 Why did this storm produce so many dancing sprites?

The present observations support the hypothesis proposed by van der Velde et al. (2014) that dancing sprites occur in storms where the stratiform precipitation regions are large enough to accommodate sequences of large scale negative leader developments. When the stratiform region is large enough and has high enough charge density the cut-off section of the branch can produce a CMC high enough to trigger a sprite. Since it takes time to develop a large stratiform region, dancing sprites should primarily occur in long duration storms. Negative leader development is determined by positive charge in front of it. Thus, there must be a large positive potential in the stratiform region that drives the leaders. Lu et al. (2013) and Bór et al. (2018) suggest that localized positive charge concentrations in the stratiform are responsible for the current surges that trig-

ger sprites, since the negative leaders will experience intense branching and acceleration in their vicinity. In this storm, such regions are implied by the structure of higher radar reflectivity in the stratiform region seen in Figure 9 and by the long propagation of the flashes across the stratiform region and the multiple ground strokes of both polarities. Thus, the large proportion of dancing sprites in this storm could be related to the long lifetime in combination with strong convective conditions. These could be a favorable criterion for a complex charge structure in the stratiform region with large positive potential and pockets of both positive and negative charge driving the leaders and allowing +CG strokes to discharge substantial amounts of charge.

6.5 Conclusion

This study considered a long duration MCS ($\sim$ 20 hours) on 21st September 2019 that produced 21 sprites captured on video of which 19 were of dancing type. The SP+CG flashes and strokes responsible for the sprite initiation, and the whole lightning activity of the storm were analyzed using Radio-Frequency radiations from a VHF LMA, LF and VLF detections from two operational LLS, and CMWs from ELF receiver measurements. CTT and radar data as well as meteorological reanalysis data allowed a comprehensive analysis of the cloud conditions that generated the high amount of dancing sprites.

We find that the SP+CG flashes were of exceptionally long horizontal extent and duration (average of 156 km and 2.9 seconds, respectively), that is, 3-4 times longer than previously reported values from LMA-based studies.The flashes that triggered the dancing sprites followed a similar propagation pattern where most flashes initiated in the convective region of an asymmetric MCS with a bow echo phase and propagated into the stratiform region. Here, the flashes followed paths of higher radar reflectivity ($\geq$ 35 dBZ) and produced several +CG strokes that triggered sprites, after a mechanism that resembles "cutoff of negative leader". The flash initiation regions as well as the altitude of propagation of leaders during sprite production change with the storm evolution, indicating variations in convective cell activity with time and a lowering of the positive charge region as the storm dissipates, respectively. Most sprite sequences (87.5%) were produced by distinct +CG strokes separated in time by tens to hundreds of milliseconds (80 % were between 40 and 300 ms). However, in the case studies we find two sprite sequences, each triggered with a short delay after three strokes separated by a very short time (1-3 ms) and a large distance (spanning 32-54 km). We argue that this could be a new type of dancing sprite in which the individual sequences are not resolvable at video frame rates of 25 frames/second leading to exceptionally wide and bright sprites that do not match any of the currently reported categories of sprite morphology.

We investigated the meteorological conditions that lead to a high proportion of dancing sprites and conclude that this was associated to the convective conditions in which the storm developed with extreme CAPE values of 3,500 J kg^{-1} and wind shear of 20 m s^{-1}, resulting in a large region with cold CTT (2,900 km^2 with CTT < -66°C) and a high maximum CG flash rate (30-35 fl min^{-1}). We hypothesize that the long lifetime of the storm, the complex and rapidly evolving convective charge structure that resembled an inverted dipole during the phase of a bow echo, and the development of the extensive stratiform region with a large amount of charge of both polarities, could be related to these conditions. This enabled the SP+CG flashes to propagate over large distances from convective to stratiform regions and reverse, producing multiple +CG strokes. The +CG strokes discharged substantial amounts of charge in a sequential manner that is reflected above the storm by triggering a sequence of sprites that appears to be dancing.

Acknowledgments

The authors thank the French AERIS/ICARE Data and Services Center which provided MSG/SEVIRI data for cloud top temperature. They thank also the European Copernicus/ECMWF Data Center, the US NCEP/NCAR and NOAA for providing meteorological reanalysis. The authors thank the companies Météorage and Vaisala which provided the CG lightning activity data. The Instrument National d'Excellence (INE) SAETTA network is supported by CNES, CNRS and Collectivité de Corse (`https://saetta.aeris-data.fr/`). Observation data were collected at the Pyrenean Platform for Observation of the Atmosphere P2OA (`http://p2oa.aero.obs-mip.fr`). P2OA facilities and staff are funded and suported by the University Paul Sabatier, Toulouse, France, and CNRS (Centre National de la Recherche Scientifique). P2OA is a component of the ACTRIS-Fr Research Infrastructure and benefits from AERIS data center (`https://www.aeris-data.fr/`) for hosting service data. This study was partially supported by the ANR EXAEDRE (ANR-16-CE04-0005) and CNES SOLID projects. JM acknowledges the support of the National Science Centre, Poland, under grant 2015/19/B/ST10/01055. The authors would like to thank the three anonymous reviewers whose comments helped to improve the paper. **Data Availability:** The data used for this publication can be obtained from DOI:10.5281/zenodo.4916043. The GLD360 data are from 2019-09-21 04-24 UTC in the region lat: 39-44 N lon: 0-12 E and can be requested by contacting Vaisala at Thunderstorm.support@vaisala.com.

References

Bór, J. (2013). Optically perceptible characteristics of sprites observed in Central Europe in 2007-2009. *Journal of Atmospheric and Solar-Terrestrial Physics*, *92*, 151–177. doi: 10.1016/j.jastp.2012.10.008

Bór, J., Zelkó, Z., Hegedüs, T., Jäger, Z., Mlynarczyk, J., Popek, M., & Betz, H. D. (2018). On the Series of +CG Lightning Strokes in Dancing Sprite Events. *Journal of Geophysical Research: Atmospheres*, *123*(19), 11030–11047. doi: 10.1029/2017JD028251

Braun, S., & Houze, R. A. (1994). The transition zone and secondary maximum of radar reflectivity behind a mid-latitude squall line: Results retrieved from Doppler radar data. *J. Atmos. Sci.*, *51*, 2733–2755.

Carey, L. D., Murphy, M. J., McCormick, T. L., & Demetriades, N. W. (2005). Lightning location relative to storm structure in a leading-line, trailing-stratiform mesoscale convective system. *Journal of Geophysical Research: Atmospheres*, *110*(3), 1–23. doi: 10.1029/2003JD004371

Coquillat, S., Defer, E., Guibert, P. D., Lambert, D., Pinty, J.-p., Pont, V., ... Rison, W. (2019). SAETTA : high-resolution 3-D mapping of the total lightning activity in the Mediterranean Basin over Corsica , with a focus on a mesoscale convective system event. *Atmospheric Measurement Techniques*, *12*, 5765–5790. doi: 10.5194/amt-12-5765-2019

Cummer, S. A. (2003). Current moment in sprite-producing lightning. *Journal of Atmospheric and Solar-Terrestrial Physics*, *65*(5), 499–508. doi: 10.1016/S1364-6826(02)00318-8

Cummer, S. A., & Füllekrug, M. (2001). Unusually intense continuing current in lightning produces delayed mesospheric breakdown. *Geophysical Research Letters*, *28*(3), 495–498.

Cummer, S. A., Inan, U. S., Bell, T. F., & Barrington-Leigh, C. P. (1998). ELF radiation produced by electrical currents in sprites. *Geophysical Research Letters*, *25*(8), 1281–1284. doi: doi:10.1029/98GL50937

Dye, J. E., & Bansemer, A. (2019). Electrification in Mesoscale Updrafts of Deep Stratiform and Anvil Clouds in Florida. *Journal of Geophysical Research: Atmospheres*, *124*(2), 1021–1049. doi: 10.1029/2018JD029130

Farges, T., & Blanc, E. (2011). Champs électriques induits par les éclairs et les événements lumineux transitoires et leur effet sur l'ionosphère. *Comptes Rendus Physique*, *12*(2), 171–179. doi: 10.1016/j.crhy.2011.01.013

Fuchs, B. R., Bruning, E. C., Rutledge, S. A., Carey, L. D., Krehbiel, P. R., & Rison, W. (2016, 7). Climatological analyses of LMA data with an open-source lightning flash-clustering algorithm. *Journal of Geophysical Research*, *121*(14), 8625–8648. doi: 10.1002/2015JD024663

Gomez Kuri, Z., Soula, S., Neubert, T., Mlynarczyk, J., & Köhn, C. (2021). Converging Luminosity in Column-Sprite Filaments. *Geophysical Research Letters*, *48*. doi: 10.1029/2020GL090364

Houze, R. A., Smull, B. F., & Dodge, P. (1990). Mesoscale organization of springtime rainstorms in Oklahoma. *Mon. Weather Rev*, *118*.

Inan, U. S., Cummer, S. A., & Marshall, R. A. (2010). A survey of ELF and VLF research on lightning-ionosphere interactions and causative discharges. *Journal of Geophysical Research: Space Physics*, *115*(6), 1–21. doi: 10.1029/2009JA014775

Jacobson, M. Z. (2005). *Fundamentals of atmospheric modeling (2nd edition)* (2nd ed., Vol. 9780521839). Cambridge University Press. doi: 10.1017/CBO9781139165389

Kolmašová, I., Santolík, O., Farges, T., Cummer, S. A., Lán, R., & Uhlíř, L. (2016). Subionospheric propagation and peak currents of preliminary breakdown pulses before negative cloud-to-ground lightning discharges. *Geophys. Res. Lett.*, *43*(16), 1–8. doi: 10.1002/2015GL067364

Krehbiel, P. R. (1981). *An analysis of the electric field change produced by lightning [Ph.D. dissertation]*. Univ. of Manchester Inst. of Science and Technology.

Lang, T. J., Lyons, W. A., Cummer, S. A., Fuchs, B. R., Dolan, B., Rutledge, S. A., ... Ashcraft, T. (2016). Observations of two sprite-producing storms in Colorado. *Journal of Geophysical Research*, *121*(16), 9675–9695. doi: 10.1002/2016JD025299

Lang, T. J., Lyons, W. A., Rutledge, S. A., Meyer, J. D., MacGorman, D. R., & Cummer, S. A. (2010). Transient luminous events above two mesoscale convective systems: Storm structure and evolution. *Journal of Geophysical Research: Space Physics*, *115*(5), 1–22. doi: 10.1029/2009JA014500

Lang, T. J., & Rutledge, S. A. (2008). Kinematic, microphysical, and electrical aspects of an asymmetric bow-echo mesoscale convective system observed during STEPS 2000. *Journal of Geophysical Research Atmospheres*, *113*(8), 1–21. doi: 10.1029/2006JD007709

Lang, T. J., Rutledge, S. A., & Wiens, K. C. (2004). Origins of positive cloud-to-ground lightning flashes in the stratiform region of a mesoscale convective system. *Geophysical Research Letters*, *31*(10). doi: 10.1029/2004GL019823

Li, J., Cummer, S. A., Lyons, W. A., & Nelson, T. E. (2008). Coordinated analysis of delayed sprites with high-speed images and remote electromagnetic fields. *Journal of Geophysical Research Atmospheres*, *113*(20), 1–11. doi: 10.1029/2008JD010008

Lu, G., Cummer, S. A., Li, J., Han, F., Blakeslee, R. J., & Christian, H. J. (2009). Charge transfer and in-cloud structure of large-charge-moment positive lightning strokes in a mesoscale convective system. *Geophysical Research Letters*, *36*(15), 1–5. doi: 10.1029/2009GL038880

Lu, G., Cummer, S. A., Li, J., Zigoneanu, L., Lyons, W. A., Stanley, M. A., ... Samaras, T. (2013). Coordinated observations of sprites and in-cloud lightning flash structure. *Journal of Geophysical Research Atmospheres*, *118*(12), 6607–6632. doi: 10.1002/jgrd.50459

Lyons, W. A. (1994). Characteristics of luminous structures in the stratosphere above thunderstorms as imaged by low-light video. *Geophysical Research Letters*, *21*(10), 875–878. doi: 10.1029/94GL00560

Lyons, W. A. (1996). Sprite observations above the U.S. High Plains in relation to their parent thunderstorm systems. *Journal of Geophysical Research Atmospheres*, *101*(23), 29641–29652. doi: 10.1029/96jd01866

Lyons, W. A., Nelson, T. E., Williams, E. R., Cummer, S. A., & Stanley, M. A. (2003). Characteristics of sprite-producing positive cloud-to-ground lightning during the 19 July 2000 STEPS mesoscale convective systems. *Monthly Weather Review*, *131*(10), 2417–2427. doi: 10.1175/1520-0493(2003)131<2417:COSPCL>2.0.CO;2

Ma, Z., Jiang, R., Qie, X., Xing, H., Liu, M., Sun, Z., ... Li, X. (2021, 2). A low frequency 3D lightning mapping network in north China. *Atmospheric Research*, *249*, 105314. doi: 10.1016/j.atmosres.2020.105314

Mallick, S., Rakov, V. A., Hill, J. D., Ngin, T., Gamerota, W. R., Pilkey, J. T., ... Nag, A. (2014). Performance characteristics of the NLDN for return strokes and pulses superimposed on steady currents, based on rocket-triggered lightning data acquired. *Journal of Geophysical Research: Atmospheres*, *119*, 3825–3856. doi: 10.1002/2013JD021401

McHarg, M. G., Stenbaek-Nielsen, H. C., & Kammae, T. (2007). Observations of streamer formation in sprites. *Geophysical Research Letters*, *34*(6), 1–5. doi: 10.1029/2006GL027854

Mlynarczyk, J., Bór, J., Kulak, A., Popek, M., & Kubisz, J. (2015). An unusual sequence of sprites followed by a secondary TLE: An analysis of ELF radio measurements and optical observations. *Journal of Geophysical Research: Space Physics*, *120*, 2241–2254. doi: 10.1002/2014JA020780

Montanya, J., van der Velde, O., Solà, G., Fabró, F., Romero, D., Pineda, N., & Argemí, O. (2014). Lightning flash properties derived from Lightning Mapping Array data. *2014 International Conference on Lightning Protection*, 974–978. doi: 10.1109/ICLP.2014.6973264

Nag, A., & Rakov, V. A. (2012). Positive lightning: An overview, new observations, and inferences. *Journal of Geophysical Research Atmospheres*, *117*(8), 1–20. doi: 10.1029/2012JD017545

Neubert, T., Rycroft, M., Farges, T., Blanc, E., Chanrion, O., Arnone, E., ... Crosby, N. (2008). Recent results from studies of electric discharges in the mesosphere. *Surveys in Geophysics*, *29*(2), 71–137. doi: 10.1007/s10712-008-9043-1

Pasko, V. P., Inan, U. S., Bell, T. F., & Taranenko, Y. N. (1997). Sprites produced by quasi-electrostatic heating and ionization in the lower ionosphere. *Journal of Geophysical Research: Space Physics*, *102*(A3), 4529–4561. doi: 10.1029/96JA03528

Pedeboy, S. (2015). Analysis of the French lightning locating system location accuracy. *2015 International Symposium on Lightning Protection, XIII SIPDA 2015*, 337–341. doi: 10.1109/SIPDA.2015.7339299

Qin, J., Celestin, S., & Pasko, V. P. (2013). Dependence of positive and negative sprite morphology on lightning characteristics and upper atmospheric ambient conditions. *Journal of Geophysical Research: Space Physics*, *118*(5), 2623–2638. doi: 10.1029/2012JA017908

Rison, W., Thomas, R. J., Krehbiel, P. R., Hamlin, T., & Harlin, J. (1999, 12). A GPS-based three-dimensional lightning mapping system: Initial observations in central New Mexico. *Geophysical Research Letters*, *26*(23), 3573–3576. doi: 10.1029/1999GL010856

Said, R. K., Inan, U. S., & Cummins, K. L. (2010). Long-range lightning geolocation using a VLF radio atmospheric waveform bank. *Journal of Geophysical Research Atmospheres*, *115*(23), 1–19. doi: 10.1029/2010JD013863

Said, R. K., & Murphy, M. J. (2016). GLD360 Upgrade: Performance Analysis and Applications. In *24th international lightning detection conference.*

São Sabbas, F. T., Sentman, D. D., Wescott, E. M., Pinto, O., Mendes, O., & Tay-

lor, M. J. (2003). Statistical analysis of space-time relationships between sprites and lightning. *Journal of Atmospheric and Solar-Terrestrial Physics*, *65*(5), 525–535. doi: 10.1016/S1364-6826(02)00326-7

São Sabbas, F. T., Taylor, M. J., Pautet, P.-D., Bailey, M., Cummer, S., Azambuja, R. R., ... Conforte, J. C. (2010). Observations of prolific transient luminous event production above a mesoscale convective system in argentina during the sprite2006 campaign in brazil. *Journal of Geophysical Research: Space Physics*, *115*(A11). doi: https://doi.org/10.1029/2009JA014857

Schulz, W., Diendorfer, G., Pedeboy, S., & Roel Poelman, D. (2016). The European lightning location system EUCLID - Part 1: Performance analysis and validation. *Natural Hazards and Earth System Sciences*, *16*(2), 595–605. doi: 10.5194/nhess-16-595-2016

Sentman, D., Wescott, E. M., Osborne, D., Hampton, D., & Heavner, M. (1995). Preliminary results from the Sprites94 Aircraft Campaign: 2. Blue jets. *Geophysical Research Letters*, *22*(10), 1209–1212. doi: 10.1029/95GL00582

Shao, X. M., & Krehbiel, P. R. (1996, 11). The spatial and temporal development of intracloud lightning. *Journal of Geophysical Research Atmospheres*, *101*(21), 26641–26668. doi: 10.1029/96jd01803

Soula, S., Defer, E., Füllekrug, M., van der Velde, O., Montanya, J., Bousquet, O., ... Pedeboy, S. (2015). Time and space correlation between sprites and their parent lightning flashes for a thunderstorm observed during the HyMeX campaign. *Journal of Geophysical Research*, *120*(22), 11552–11574. doi: 10.1002/2015JD023894

Soula, S., Iacovella, F., van der Velde, O., Montanyà, J., Füllekrug, M., Farges, T., ... Martin, J. M. (2014). Multi-instrumental analysis of large sprite events and their producing storm in southern France. *Atmospheric Research*, *135-136*, 415–431. doi: 10.1016/j.atmosres.2012.10.004

Soula, S., Mlynarczyk, J., Füllekrug, M., Pineda, N., Georgis, J. F., van der Velde, O., ... Fabró, F. (2017). Dancing sprites: Detailed analysis of two case studies. *Journal of Geophysical Research*, *122*(6), 3173–3192. doi: 10.1002/2016JD025548

Soula, S., van der Velde, O., Montanyà, J., Neubert, T., Chanrion, O., & Ganot, M. (2009). Analysis of thunderstorm and lightning activity associated with sprites observed during the EuroSprite campaigns: Two case studies. *Atmospheric Research*, *91*(2-4), 514–528. doi: 10.1016/j.atmosres.2008.06.017

Stanley, M., Krehbiel, P., Brook, M., Moore, C., Rison, W., & Abrahams, B. (1999). High speed video of initial sprite development. *Geophysical Research Letters*, *26*(20), 3201–3204. doi: 10.1029/1999GL010673

Stenbaek-Nielsen, H. C., & McHarg, M. G. (2008). High time-resolution sprite imaging: Observations and implications. *Journal of Physics D: Applied Physics*, *41*(23). doi: 10.1088/0022-3727/41/23/234009

Thomas, R. J., Krehbiel, P. R., Hamlin, T., Harlin, J., & Shown, D. (2001). Observations of VHF source powers radiated by lightning. *Geophysical Research Letters*, *28*(1), 143–146. doi: 10.1029/2000GL011464

Thomas, R. J., Krehbiel, P. R., Rison, W., Hunyady, S. J., Winn, W. P., Hamlin, T., & Harlin, J. (2004). Accuracy of the lightning mapping array. *Journal of Geophysical Research: Atmospheres*, *109*(14), 1–34. doi: 10.1029/2004JD004549

van der Velde, O. A., Bór, J., Li, J., Cummer, S. A., Arnone, E., Zanotti, F., ... Farges, T. (2010). Multi-instrumental observations of a positive gigantic jet produced by a winter thunderstorm in Europe. *Journal of Geophysical Research Atmospheres*, *115*(24), 1–17. doi: 10.1029/2010JD014442

van der Velde, O. A., Mika, Ã., Soula, S., Haldoupis, C., Neubert, T., & Inan, U. S. (2006). Observations of the relationship between sprite morphology and incloud lightning processes. *Journal of Geophysical Research Atmospheres*, *111*(15). doi: 10.1029/2005JD006879

van der Velde, O. A., & Montanyà, J. (2013). Asymmetries in bidirectional leader development of lightning flashes. *Journal of Geophysical Research Atmospheres*, *118*(24), 13504–13519. doi: 10.1002/2013JD020257

van der Velde, O. A., Montanyà, J., Soula, S., Pineda, N., & Bech, J. (2010). Spatial and temporal evolution of horizontally extensive lightning discharges associated with sprite-producing positive cloud-to-ground flashes in northeastern Spain. *Journal of Geophysical Research: Space Physics*, *115*(9), 1–17. doi: 10.1029/2009JA014773

van der Velde, O. A., Montanyà, J., Soula, S., Pineda, N., & Mlynarczyk, J. (2014). Bidirectional leader development in sprite-producing positive cloud-to-ground flashes: Origins and characteristics of positive and negative leaders. *Journal of Geophysical Research: Atmospheres*, *119*. doi: 10.1002/2013JD021291

Winckler, J. R., Lyons, W. A., Nelson, T. E., & Nemzek, R. J. (1996). New high-resolution ground-based studies of sprites. *Journal of Geophysical Research Atmospheres*, *101*(D3), 6997–7004. doi: 10.1029/95JD03443

Yang, J., Lu, G., Lee, L. J., & Feng, G. (2015). Long-delayed bright dancing sprite with large Horizontal displacement from its parent flash. *Journal of Atmospheric and Solar-Terrestrial Physics*, *129*, 1–5. doi: 10.1016/j.jastp.2015.04.001

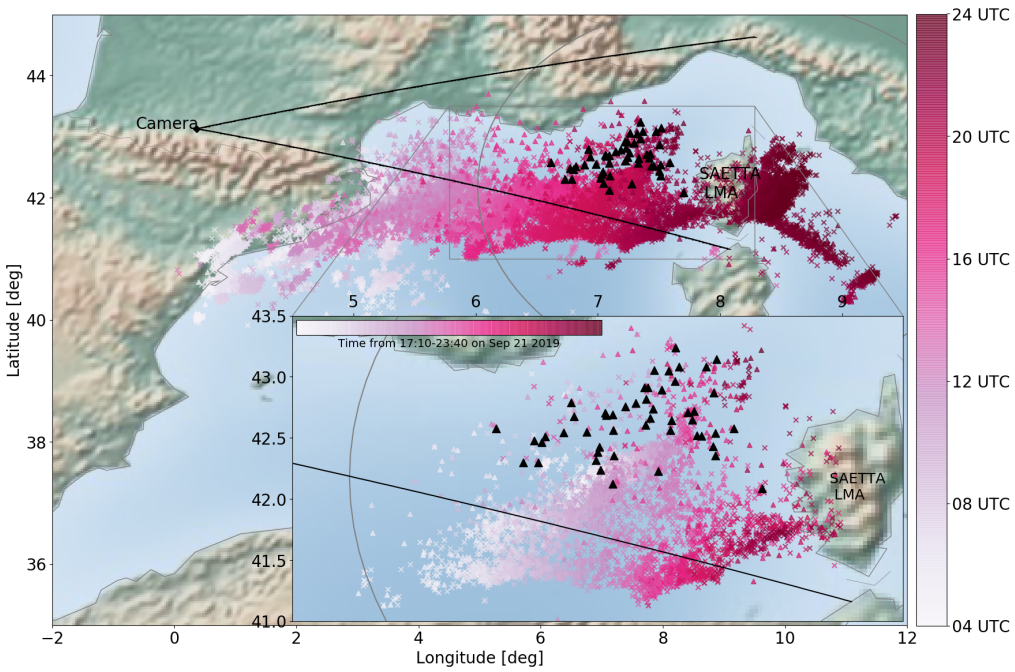

Figure 1. CG lightning flashes detected by GLD360 on September 21, 2019, from 04:00-24:00 UTC in the west Mediterranean are plotted with colored crosses (-CG) and triangles (+CG). The color indicates time (from earliest=light to latest=dark). The SP+CG strokes identified in MTRG data are plotted with black triangles. The SAETTA domain of interest (grey circle), the camera location and the horizontal FOV of the camera (black lines) are also shown. The zoomed inset shows the CG activity recorded during the period of the sprites studied here (17:10-23:40 UTC) and within their domain of occurrence.

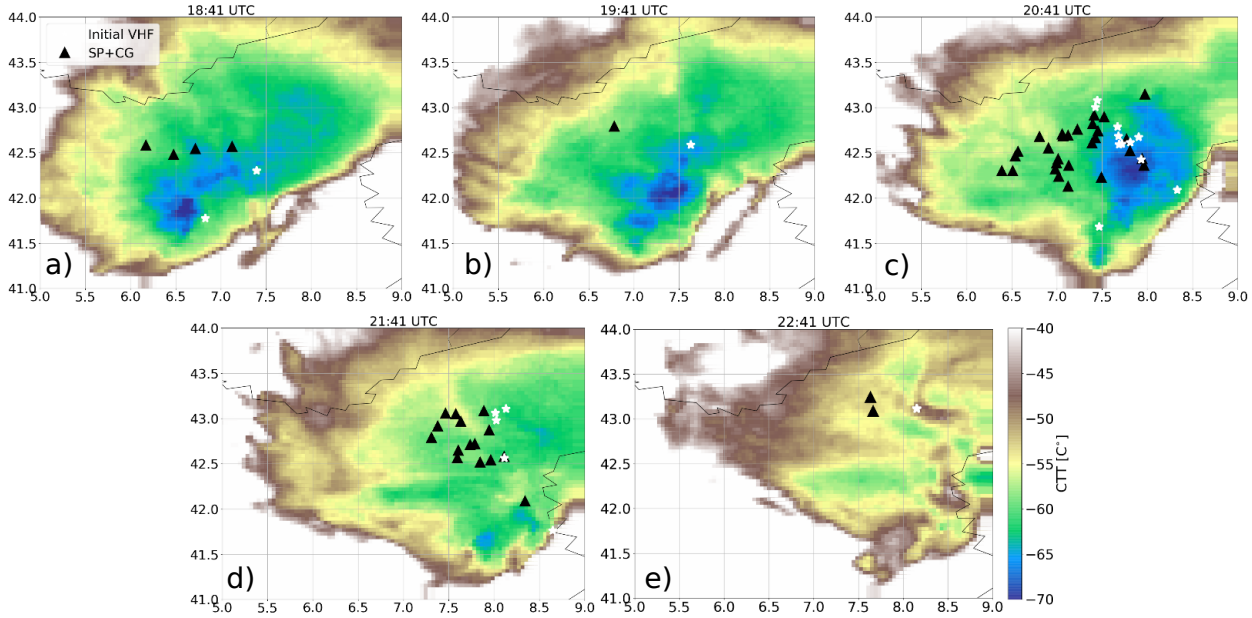

Figure 2. Five (a-e) snapshots of CTT during the last (and sprite producing) period of the storm lifetime. The SP+CG strokes reported by MTRG from one hour around the time of the respective SEVIRI scan are plotted as black triangles. White stars show the location of flash initiation retrieved from the SAETTA LMA records for each SP+CG flash.

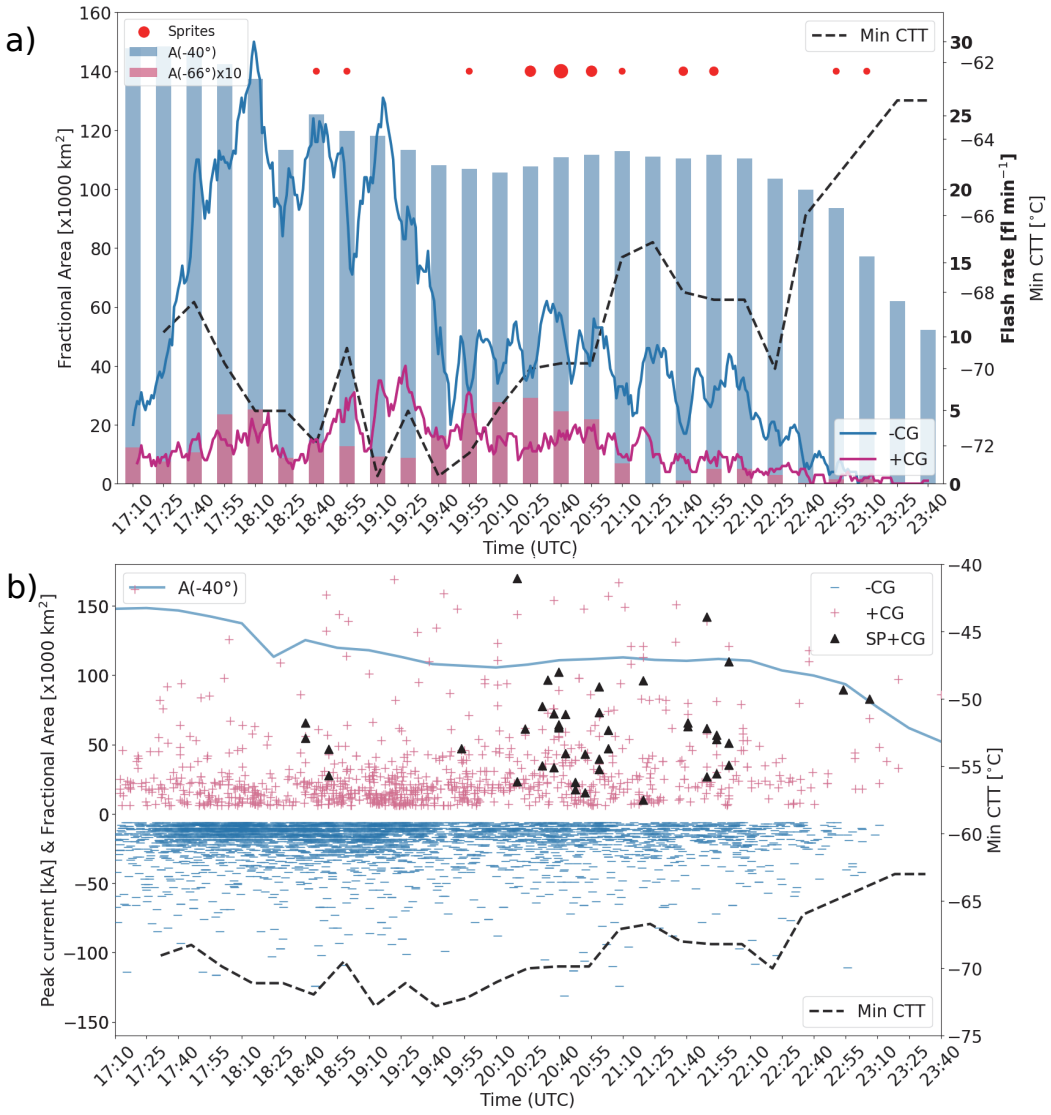

Figure 3. a) Time evolution of storm characteristics during the sprite producing part of the storm. Blue bars: Fractional storm area A(-40°). Pink bars: Fractional area of strongest convection A(-66°) multiplied by 10 for scale. Black dashed line: Minimum CTT. Red circles: Sprite events within 15 minutes time slot (size represents the relative number of events). Solid lines show GLD360 CG flash rate (smoothed with 5 minutes moving average). b) Time series of the strongest peak current of each CG lightning flash as reported by GLD360. The triangles correspond to the SP+CG strokes detected by MTRG. Panel b also shows the storm size in terms of fractional area A(-40°) and the minimum CTT.

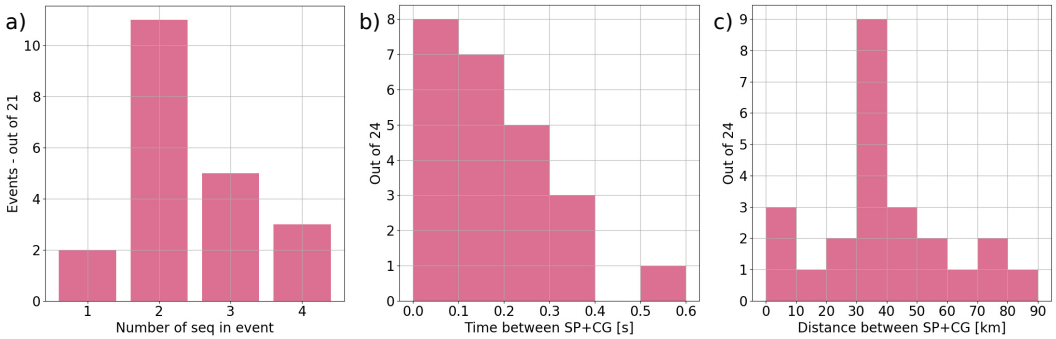

Figure 4. a) Distribution of the 21 sprite events versus the number of sequences for all 21 events. b) Time between successive SP+CG strokes in the same dancing sprite. c) Distance between successive SP+CG strokes in the same dancing sprite. In panel b) and c) the total number of data points is 24, which is the number of times two successive SP+CG strokes within one event were both identified.

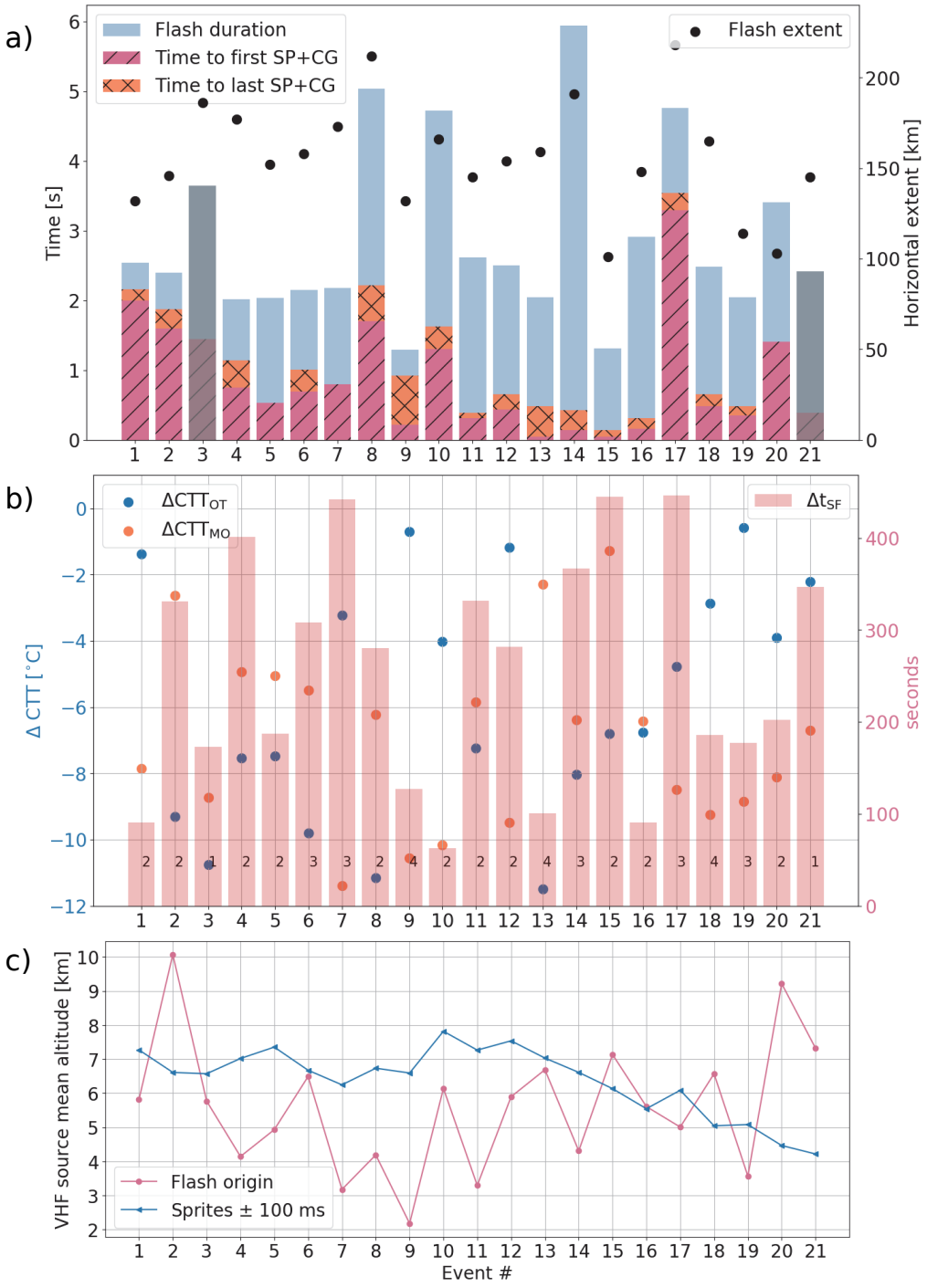

Figure 5. a) Flash duration and extent for all 21 parent flashes. Events #3 and #21 are shown in grey, since they were single sprites. The bars show flash duration, time from the first VHF source until the first SP+CG and when identified, also last SP+CG in the event. The black dots show the flash horizontal extent. b) Blue dots show the difference in CTT between flash origin and flash termination (ΔCTT_{OT}) calculated from LMA data. Orange dots display the difference in CTT between the minimum CTT at the time of the flash and the CTT at flash origin (ΔCTT_{MO}). The bars show the time difference between CTT scan and the flash initiation time (Δt_{SF}). The annotated number corresponds to the number of sprite sequences in the event. c) Mean altitude of VHF sources for flash origin and during sprite sequences (this is an average of sources measured from 100 ms before the first sprite sequence until 100 ms after the last sprite sequence. These sources are shown in orange for the three case studies in Figure 6b, 7b and 8b).

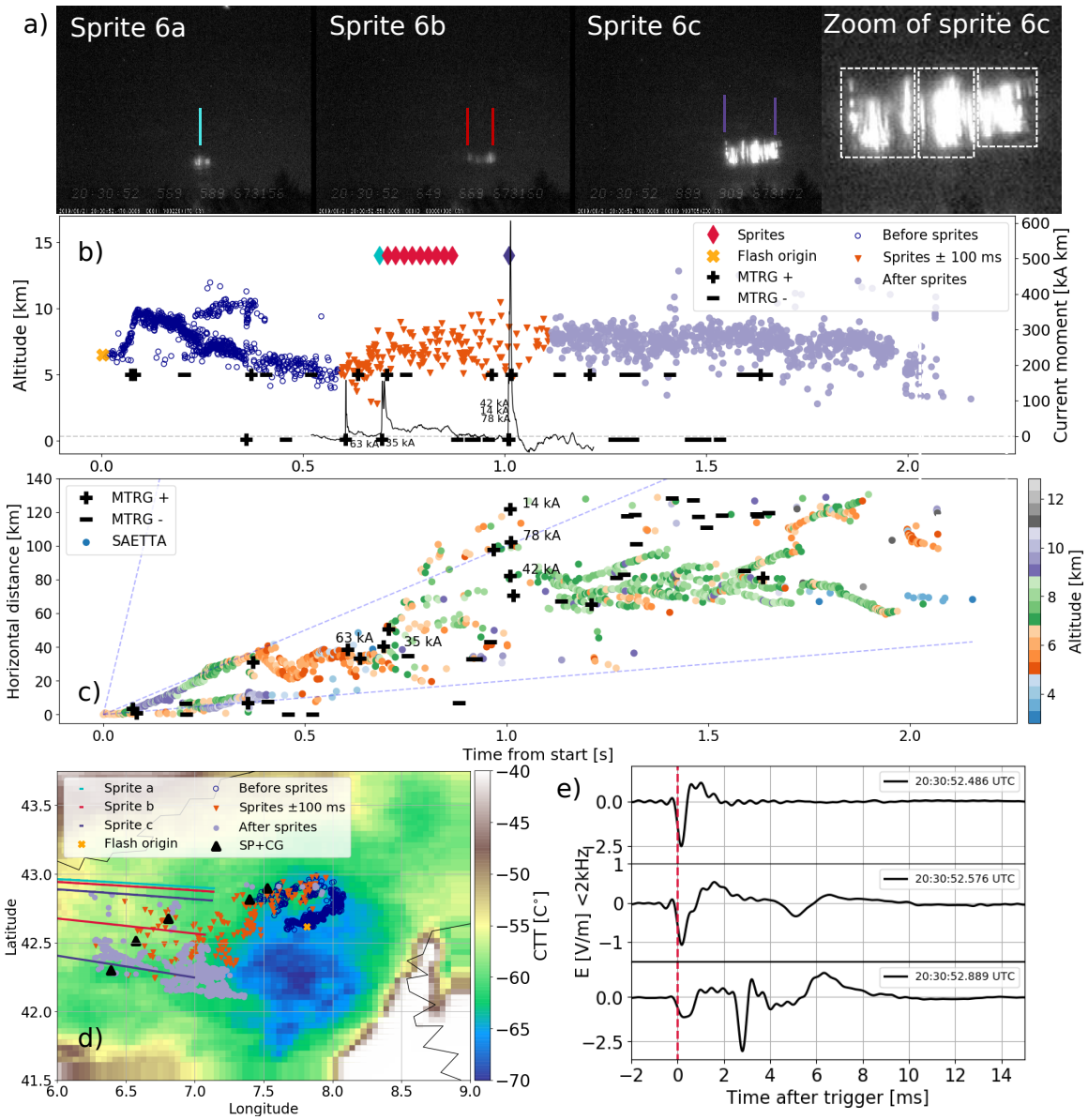

Figure 6. a) Brightest video field for each sequence in event #6 at 20:30:52 UTC, including a zoom of sprite 6c with boxes indicating three distinguishable structures. The lines (one color for each sprite) indicate the location of the LOS from the camera to the sprite reported in panel d). b) Altitude of VHF sources with time. All MTRG detections are shown as pluses and minuses (for positive and negative polarity, respectively) with IC at arbitrary altitude and CG strokes at ground level. The peak current is only annotated for the SP+CG strokes which are also listed in Table 1. Overlaid is the CMW during the sprite production (black curve). c) Time-distance plot of the parent flash with colors representing altitude. Pluses and minuses are positive and negative polarity MTRG detections. The dashed lines are reference lines for leader speeds. Going from steepest to flattest they are 10^6 m s^{-1}, 10^5 m s^{-1} (typical speed of negative leaders) and 2×10^4 m s^{-1} (typical speed for positive leaders as observed in VHF). d) Longitude-latitude map. CTT at 20:26 UTC from SEVIRI is shown in colors. The LOS direction of the sprites are shown in lines with one color for each sprite sequence as explained in the legend. VHF sources from the parent flash are superimposed. Blue open circles are from before the sprites, triangles are during the sprites, grey full circles are after the sprites. e) Vertical electric field (ELF band) during the event reconstructed from the data recorded by a broadband vertical dipole whip antenna installed in the center of France. Each legend shows the trigger time (i.e. including the signal propagation time of ∼2 ms for 700 km distance from storm to antenna) corresponding to t=0 (red dashed line).

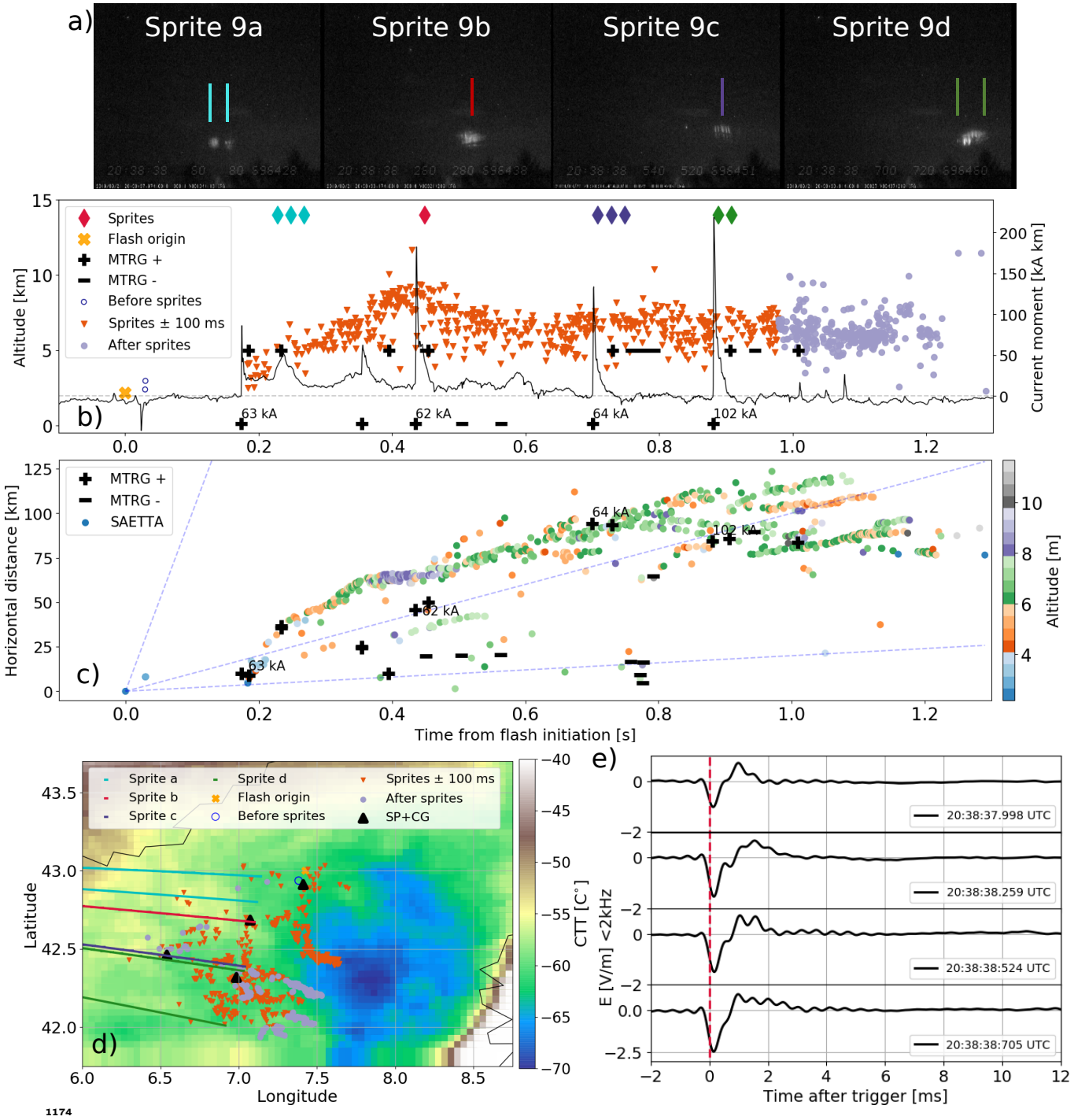

Figure 7. Same as Figure 6 but for event #9 at 20:38:38 UTC. The CTT in panel d) is measured at 20:41 UTC.

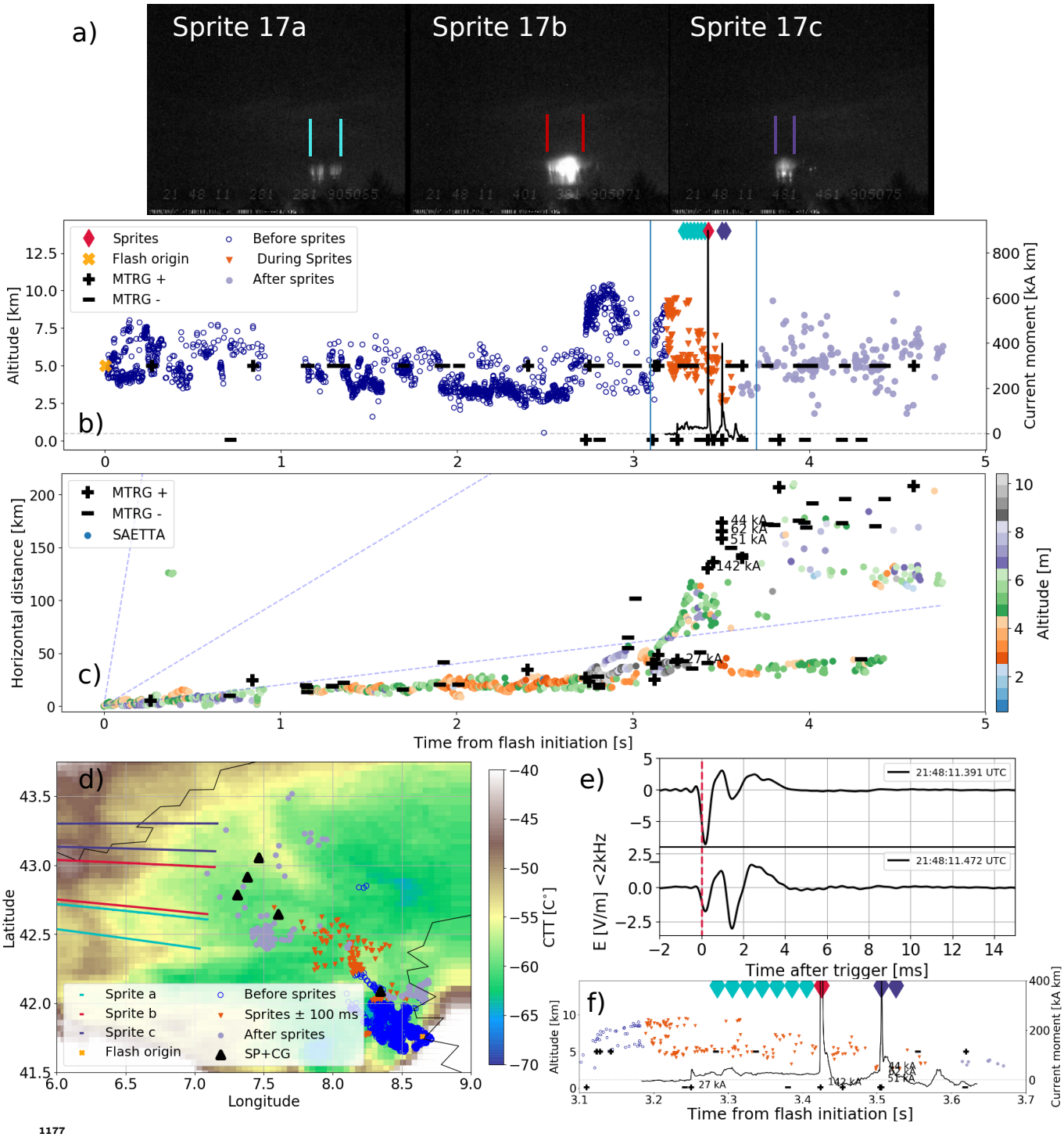

Figure 8. Same as Figure 6 but for event #17 at 21:48:11 UTC, with in f) a zoom of the CMW waveform. The temporal extent of the zoom is shown in panel b with blue vertical lines. The CTT in panel d) is measured at 21:41 UTC.

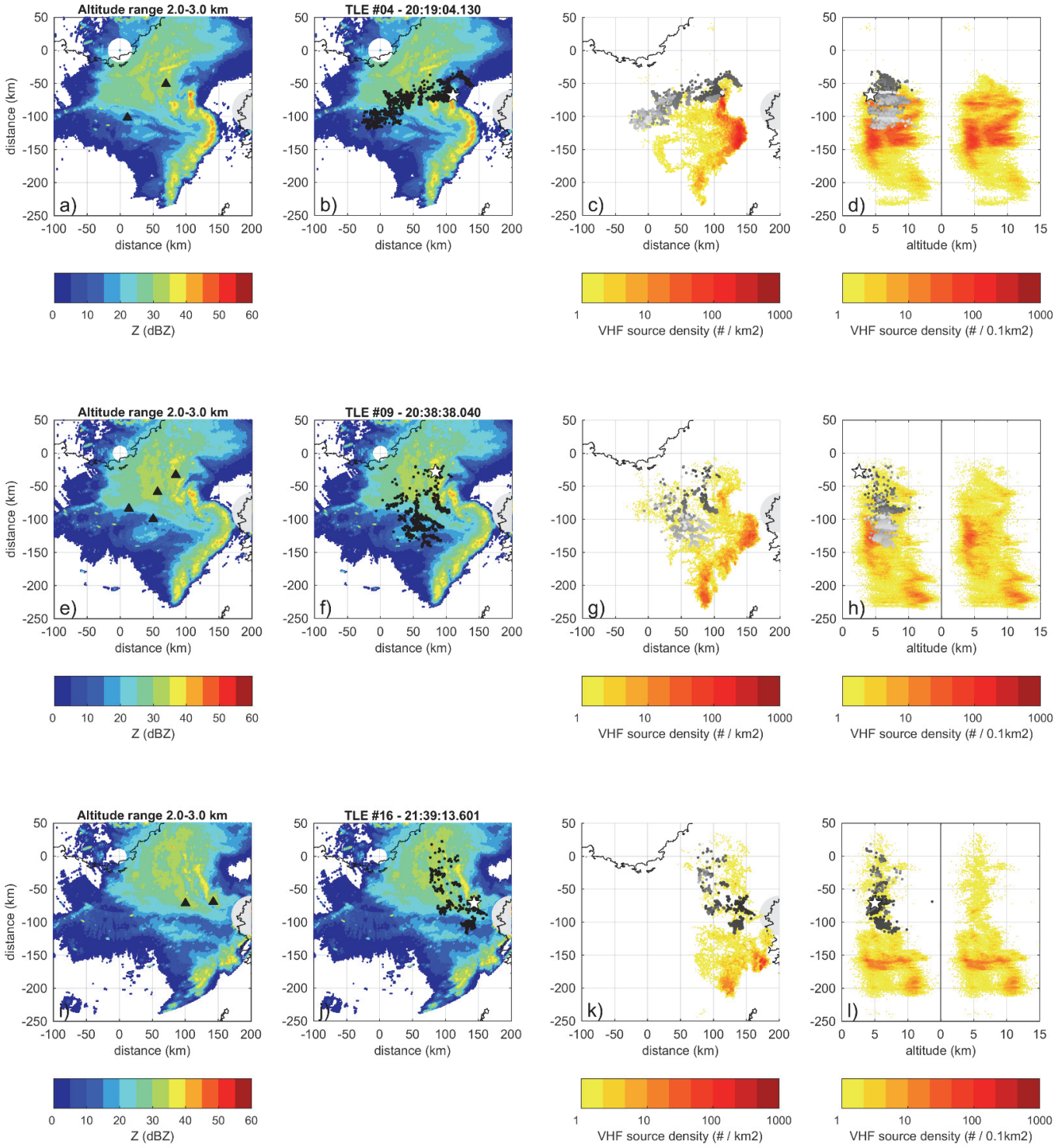

Figure 9. For the events #4, #9 and #16 the figures show: a),e),i) Radar reflectivity between 2 and 3 km altitude, with MTRG SP+CG strokes from the respective event. b),f),j) Same as a),e),i) but with an overlay of the reconstructed VHF sources with the white star showing the average location of the first three reconstructed VHF sources. c),g),k) Projection of the VHF source density for 10 minutes around the event (9 minutes before and 1 minute after) computed for a 1 km x 1 km grid mesh. Overlay of the reconstructed VHF sources of the SP+CG flash in greyscale as a function of time where grey colors span from dark-grey to light-grey from the beginning to the end of the flash duration. d),h),l) VHF source density projected along the altitude and the distance North-South per 0.1 km x 1 km bin, plotted twice side by side, in one with the altitude-latitude overlay of the parent flash.